BLIND SOURCE SEPARATION AND LOCALIZATION USING MICROPHONE ARRAYS

By

LONGJI SUN

Bachelor of Engineering in Communication Engineering
University of Shanghai for Science and Technology
Shanghai, China
2010

Submitted to the Faculty of the
Graduate College of
Oklahoma State University
in partial fulfillment of
the requirements for
the Degree of
MASTER OF SCIENCE
December, 2012

BLIND SOURCE SEPARATION AND LOCALIZATION USING MICROPHONE ARRAYS

Thesis Approved:

Dr. Qi Cheng

Thesis Advisor

Dr. Weishua Sheng

Dr. Martin T. Hagan

Dr. Sheryl A. Tucker

Dean of the Graduate College

TABLE OF CONTENTS

LIST OF TABLES

Table Page

LIST OF FIGURES

CHAPTER 1

INTRODUCTION

1.1 Background

Blind source separation (BSS) recovers original source signals from collected signal mixtures and is encountered in various signal processing areas, including telecommunications, biology, image, and sonar/radar. Being "blind" means the lack of the knowledge of signal mixing process, such as mixing coefficients and signal locations. In biomedical signal processing, brain activity recordings, such as electroencephalogram (EEG) and magnetoencephalogram (MEG) data, are the combinations of brain signals of interest. BSS estimates the underlying signals which provide valuable information about human health [2]. In astronomical image processing, images from ground-based image systems are usually the mixtures of the blur from the atmosphere and the extraterrestrial objects we want to observe. BSS relieves the effect of the blur and recovers more accurate images about the objects.

The most studied BSS signals are audio signals. The well-known "cocktail party problem" is an example of blind audio source separation where the mixtures of vari-

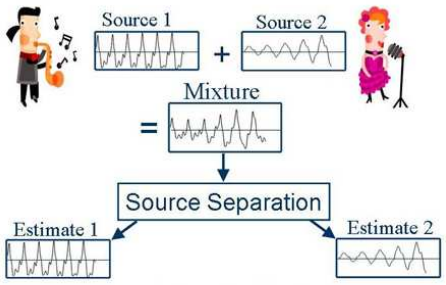

Figure 1.1: A blind source separation example.

ous sounds are given to recover the original sounds [3]. Figure 1.1 shows such a BSS example for audio signals. BSS is usually an essential preprocessing step for numerous applications. In hearing aid systems, BSS estimates original sound signals from mixtures, enhances desired signals, and suppresses undesired noise and interferences [4]. In speech recognition, source signals are firstly separated and relevant features, such as Mel frequency cepstral coefficients (MFCCs), are extracted to perform the recognition [5]. In smart home design for elderly people, human sounds are separated from environmental sounds, e.g., TV sounds, and used to recognize corresponding human activities, like coughs and speeches. In traffic scene analysis, accident crash sounds can be separated from other sounds, such as car horn sounds and passing-by sounds, so that potential accidents can be identified. In robotics, robots recognize and response to human voice commands after the received mixtures are separated. In an automatic music transcription system, after BSS performs noise reduction, the processed music data are fed into the transcription step [6].

In various situations, location information of audio sources also plays an important role. For example, the knowledge about human positions may lead robots to approaching the human subjects to provide a better service. Similarly, in the traffic scene analysis, the coordinates of accidents can help emergency services locate potentially injured persons more easily. In video conference systems, camera field of views can be adjusted accordingly based on the sound source locations, which further facilitates the separation process.

1.1.1 Categories of Blind Source Separation Problems

In BSS, mixtures can be divided into three categories based on their relation with original signals: instantaneous mixtures, pure delay mixtures, and convolutive mixtures. In the instantaneous mixture case, it is assumed that the collected mixtures are linear combinations of original source signals without considering any delay. The

spatial distances between source locations and sensor locations are ignored. While it is generally not realistic in real world situations, it usually acts as a starting point in the evaluation process of a BSS algorithm.

As to the pure delay mixtures, the mixtures are linear combinations of pure delay copies of the original source signals. That is, for each sensor observation, only the signal copy with the delay corresponding to the line of sight path between the source and the sensor is taken into account. This is generally a reasonably realistic model in open outdoor environments, where there is little reverberation and no echoes.

The convolutive mixtures are a generalization of the previous two types. The mixtures collected by each microphone are considered to be linear combinations of more than one copy of the original source signals with various delays. In other words, the signal copies with time lags corresponding to numerous paths between one sensor and one source are taken into consideration. In indoor environments, the reverberation cannot be ignored and the impulse response between one source and one sensor is modeled as a finite impulse filter with its filter length depending on room acoustics.

In terms of the relation between the number of microphones and the number of sources, the BSS can be divided into overdetermined, critically determined, and underdetermined cases. The overdetermined BSS means that there are more microphones than sources. For the critically determined BSS, the source number is equal to the microphone number, while the underdetermined BSS indicates that fewer microphones than sources are used.

1.1.2 Microphone Array Signal Processing

Microphone array signal processing has been an active research area for several decades [7]. The basic idea is that multiple microphones sample signals simultaneously to achieve the spatial diversity of source signals. Compared to radio frequency sensor arrays, the environments for microphone arrays are harsher, because audio signals are

analog and there is much reverberation in common indoor environments [8]. In our work, a subspace-based approach is used. Subspace methods take advantage of the properties of the spatial covariance matrix of received mixtures, i.e., the exploitation of the relation between the signal and noise subspaces, to localize the sources.

1.1.3 Audio Signals

Audio signals consist of speeches, music, and other kinds of sounds. The sound frequency spectrum human ears are able to detect typically ranges from about 20 Hz to nearly 20000 Hz. Audio signals are typically nonstationary, naturally broadband, and do not follow specific statistical properties. There might be many pauses and silences. Signal power might also vary a lot across time and frequency. Traditional frequency domain representation cannot capture the volatility of audio signals accurately. Several time-frequency signal representations have been proposed to address this in the literature [9]. Two commonly used representations are the short time Fourier transform (STFT) representation, also called spectrogram, and the Wigner-Ville distribution. It is known that there is a tradeoff between time and frequency resolutions in the spectrogram representation. That is, a high frequency resolution results in a low time resolution, and vice versa.

Different kinds of audio signals show different characteristics in their spectrograms. For example, speeches usually have short time durations, possess wide frequency spectrums, and may include significant unvoiced parts, while instrumental music, like piano and violin music, often comprises of harmonic frequencies.

1.2 Motivations and Main Contributions

The existing blind audio source separation and localization methods are generally time-consuming. While subspace methods have been used for source localization, the signals of interest are generally narrowband radio frequency signals. Compared

with radio frequency signals, audio signals have their own characteristics as was stated in 1.1.3, which makes it difficult, if not impossible, to directly use the existing subspace methods for narrowband radio frequency signals to solve the localization for audio signals.

Our contributions include several aspects:

1. For outdoor environments, our algorithm performs blind audio source separation and localization simultaneously based on incoherent broadband subspace methods using microphone arrays. We propose a frequency bin selection method to perform final direction of arrival (DOA) estimation.

2. Most importantly, we not only use comprehensive simulations to test the proposed algorithm, but also conduct real world environments to test their effectiveness and performance.

3. Our method supports real-time implementation. That is, unlike existing separation and localization methods using typically time-consuming optimization procedures, our method can locate and separate sources much faster by using subspace methods.

1.3 Outline of the Thesis

The thesis is organized as follows. In Chapter 2, we will review the existing BSS and localization literature most relevant to our work. In Chapter 3, we present the BSS and localization algorithm design procedure for outdoor environments. In Chapter 4, we use both simulations and experiments to test our method. In Chapter 5, concluding remarks and some discussion about future work are given.

CHAPTER 2

LITERATURE REVIEW

This chapter provides a review of blind source separation and localization techniques. Because of the extensive existing literature, we focus on the part most relevant to our work. Firstly, we present a brief overview of the blind source separation literature. Secondly, we talk about the existing work on source localization. Finally, the literature on simultaneous blind source separation and localization is presented.

2.1 Blind Source Separation

Blind source separation (BSS) has attracted lasting research interests in signal processing communities. Many algorithms have been developed, such as independent component analysis (ICA) [10], sparse component analysis (SCA) [11], computational auditory scene analysis (CASA) [12], and variance modeling [13].

ICA utilizes the statistical independence of different sources measured by information criteria, such as the mutual information and the entropy, to recover source signals from mixtures. The received signals are treated as instantaneous mixtures and an efficient learning algorithm is developed in [14]. When time delays and reverberations of the signals are considered, the problem is solved in the frequency domain so that the method for instantaneous mixtures in the time domain can be used. For convolutive mixtures, the frequency ICA suffers inherent scaling and permutation issues [15]. Various algorithms have been proposed to tackle these issues, see [16, 17, 18, 19]. To solve the scaling and permutation problems, the directivity pattern measure is proposed to detect the permutations, and a normalization step is taken to counteract

the scaling effect [20]. SCA takes advantage of the fact that audio signals, especially, speech signals, are sparse in the time-frequency domain. Each time-frequency point in a mixture spectrogram is labeled to belong to one source based on certain rules [21].

The performance of various BSS algorithms has been compared in the signal separation evaluation campaign [22]. The problem for instantaneous mixtures is close to be solved. If given an appropriate initialization, the variance modeling framework, such as nonnegative matrix decomposition (NMD) in [23], works better on instantaneous mixtures than conventional SCA and ICA, since it utilizes more prior information. However, it becomes inferior on live recordings, possibly because of the omnipresence of local optima in the objective function and the need of a better initialization [22]. For live recordings, i.e., collected mixtures in experimental processes, there is still some room left for improvement.

2.2 Source Localization

Using microphone arrays to localize sound sources has been studied a lot. One of the existing methods is the phase transform (PHAT) histogram method [24], which can locate multiple sources simultaneously. In [25], localization of multiple speech sources is obtained by first using sinusoidal tracks to model the speeches and then clustering the inter-channel phase differences between the dual channels of the tracks. The subspace methods, including multiple signal classification (MUSIC) [26] and estimation of signal parameters via rotational invariance technique (ESPRIT) [27], are used to estimate the directions of arrival (DOAs) of source signals. They are noise-robust at the cost of more sensors (e.g. antennas) than sources. Here, it is noted that the signals studied in [26, 27] are narrowband radio frequency signals. Audio signals and radio frequency signals are different in various aspects as was discussed in Chapter 1.

2.3 Blind Source Separation and Localization

2.3.1 Pure Delay Mixtures

In [1], the authors use an alternating least square (ALS) algorithm to estimate mixing matrices and source signals, while at the same time enforcing the Vandermonde structure on the columns of the mixing matrices. A reference sensor is chosen to eliminate the ambiguities underlying in the estimated mixing matrices. Localization of the sources is performed using time difference of arrival (TDOA).

2.3.2 Convolutive Mixtures

In [13], the authors propose a probabilistic model utilizing the interaural phase difference (IPD) and interaural level difference (ILD) to separate and localize multiple sources. The expectation-maximization (EM) algorithm is used to estimate the parameters of the model, and the masks are generated and used to separate the source signals. The sources are located using the estimated IPDs, which are related to the interaural time differences (ITDs).

In [28], simultaneous localization of multiple sources is achieved by firstly estimating the TDOAs among the sources. The TDOA estimation is formulated as a blind multiple-input multiple-output (MIMO) adaptive filter problem and is estimated using the adaptive eigenvalue decomposition (AED) algorithm. The filters are estimated by the triple-N ICA for convolutive mixtures (TRINICON) adaptation algorithm. The TDOAs are calculated accordingly. Triple-N means nonstationary, non-Gaussian, and nonwhite properties of the source signals. Non-Gaussianity is used to develop the algorithm, while nonstationary and nonwhite properties define the applicable data range used in the algorithm.

In [29], a system incorporating localization, separation, and recognitions is proposed by using CASA. IPDs and ILDs are jointly used as the features in a Gaussian

mixture model. The IPD and ILD estimation problem is turned into a missing data classification problem, which is solved by the EM algorithm. A major limitation of this method is that it demands a training step beforehand, which imposes a restriction on its applications. The details of this algorithm can be found in [30].

CHAPTER 3

DESIGN FOR OUTDOOR ENVIRONMENTS

In this chapter, we deal with blind source separation and localization in outdoor environments. We formulate the problem mathematically and present our subspace-based approach. We also discuss several issues related to our approach and their solutions. Since audio signals are generally broadband, a frequency domain approach is used. That is, audio signals are thought of as the combinations of signal components at different frequencies. We use subspace methods to estimate source angles at each frequency separately. The final direction of arrival estimates of sources are obtained based on some criterion.

3.1 Problem Formulation

A linear array with N microphones is assumed and each microphone is with a known location d_n with respect to the center of the array, for $n = 1, \cdots, N$. There are M audio sources each with direction of arrival (DOA) θ_m with respect to the center line of the microphone array, for $m = 1, \cdots, M$. Figure 3.1 shows the spatial configuration of the sources and microphones. Here, we deal with the overdetermined case, i.e., $M < N$. The M source signals are mixed and collected at microphone n with additive noise $n_n(t)$. Based on the central limit theorem (CLT), it is assumed that $\mathbf{n}(t) = [n_1(t), \cdots, n_N(t)]^T$ is zero mean white Gaussian noise across N microphones, where $\cdot^T$ is the transpose operator. The received mixture $x_n(t)$ at microphone n in an

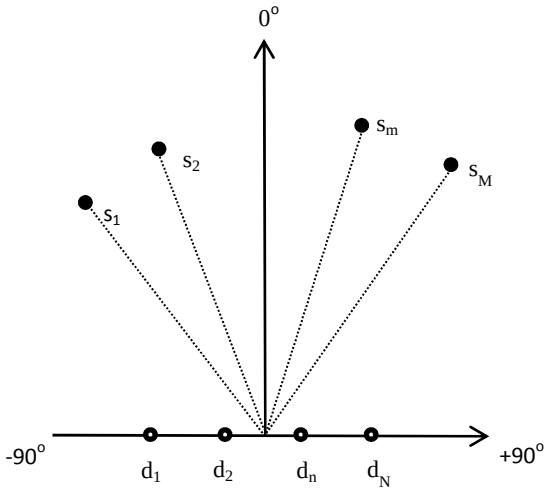

Figure 3.1: Spatial configuration of the sources and microphones.

anechoic environment can be written as:

$$x_n(t) = \sum_{m=1}^{M} a_{nm} s_m(t - \tau_{nm}) + n_n(t), \tag{3.1}$$

where a_{nm} is the attenuation coefficient between source m and microphone n, τ_{nm} is the relative arrival lag, $\tau_{nm} = d_n \sin(\theta_m)/c$, and c is the propagation velocity of sound in the medium. The direction orthogonal to the array is 0 rad, and $\theta_m \in [-\pi/2, \pi/2]$. It is also assumed that a_{nm} is uniform for all source and microphone pairs, which is generally valid in a far filed. Therefore,

$$x_n(t) = \sum_{m=1}^{M} s_m(t - \tau_{nm}) + n_n(t), \tag{3.2}$$

where t represents the continuous time.

After the sampling process and the application of a window of length K, the mixture $x_n(t)$ can be written as:

$$x_n[p, l] = \sum_{m=1}^{M} s_m([p, l] - \tau_{nm}) + n_n[p, l], \tag{3.3}$$

where p is the time frame index, and l is the discrete time index in frame p. For nonoverlapped frames, the time t for $x_n[p, l]$ is $t = [(p-1)K + l]/F_s$, where F_s is the sampling rate.

After performing the short time Fourier transform (STFT), we have

$$X_n(p,k) = \sum_{m=1}^{M} S_m(p,k) e^{-j2\pi F_s \frac{k-1}{K} \tau_{nm}} + N_n(p,k), \tag{3.4}$$

where k represents the discrete frequency index,

$$X_n(p,k) = \sum_{l=0}^{K-1} X_n[p,l] e^{-j2\pi k \frac{l}{K}}, \tag{3.5}$$

$$S_m(p,k) = \sum_{l=0}^{K-1} s_m[p,l] e^{-j2\pi k \frac{l}{K}}, \tag{3.6}$$

and

$$N_n(p,k) = \sum_{l=0}^{K-1} n_n[p,l] e^{-j2\pi k \frac{l}{K}}. \tag{3.7}$$

Due to the linearity of the STFT, the noise is also additive in the frequency domain. At frequency k, the noise at different microphones is uncorrelated, and the signals and noise are uncorrelated. In the following, we replace k with f for the clarity of representation, where $f = F_s \frac{k-1}{K}$.

The model can be written in a compact form:

$$\mathbf{X}(p,f) = \mathbf{A}(f)\mathbf{S}(p,f) + \mathbf{N}(p,f), \tag{3.8}$$

where $\mathbf{X}(p,f) = [X_1(p,f), \cdots, X_N(p,f)]^T$, $\mathbf{A}(f)$ is the $N \times M$ mixing matrix with each column $\mathbf{a}(\theta_m) = [e^{-j2\pi f d_1 \sin(\theta_m)/c}, \cdots, e^{-j2\pi f d_N \sin(\theta_m)/c}]^T$, for $1 \leq m \leq M$, and $\mathbf{S}(p,f) = [S_1(p,f), \cdots, S_M(p,f)]^T$.

The frequency-domain BSS separates the $\mathbf{X}(p,f)$ for the frequencies from 0 Hz to $F_s/2$ Hz to recover the source signals $\mathbf{s}(t)$. That is, $\widetilde{\mathbf{S}}(p,f) = \widetilde{\mathbf{W}}(f)\mathbf{X}(p,f)$, where $\widetilde{\mathbf{S}}(p,f) = [\widetilde{S}_1(p,f), \widetilde{S}_2(p,f), \cdots, \widetilde{S}_M(p,f)]^T$ is the recovered signal vector and $\widetilde{\mathbf{W}}(f)$ is the $M \times N$ estimated demixing matrix. The main objective is to perform blind source separation and localization. That is, to get the DOA estimates $\widetilde{\theta}_m$, for $m = 1, \cdots, M$, the mixing matrix estimates $\widetilde{\mathbf{A}}(f)$, the demixing matrix estimates $\widetilde{\mathbf{W}}(f)$, for $f = 0, \cdots, F_s/2$, and finally the recovered source signals $\widetilde{\mathbf{s}}(t)$ using inverse STFT.

3.2 Algorithm Design

3.2.1 Proprocessing

Before using subspace methods, the observed mixtures are normalized. That is, the processed mixture at each microphone has zero mean and unit variance. It should be emphasized that although audio signals are generally nonstationary, a short duration of the signals can be assumed to be approximately stationary. This explains why subspace methods can be applied and has been corroborated by the results of computer simulations and real world experiments.

3.2.2 Subspace Methods

The covariance matrix of $\mathbf{X}(f)$ is $\mathbf{R_{XX}}(f) = E\{\mathbf{X}(f)\mathbf{X}^H(f)\}$, where $\cdot^H$ is the conjugate transpose operator. In practice, it is approximated by the sample average $\mathbf{R_{XX}}(f) = \frac{1}{P}\sum_{p=1}^{P}\mathbf{X}(p,f)\mathbf{X}^H(p,f)$, where P is the number of frames. We can also write

$$\mathbf{R_{XX}}(f) = \mathbf{A}(f)\mathbf{R_{SS}}(f)\mathbf{A}^H(f) + \mathbf{R_{NN}}(f), \tag{3.9}$$

where $\mathbf{R_{SS}}(f) = E\{\mathbf{S}(f)\mathbf{S}^H(f)\}$.

The generalized eigenvalue decomposition is used to perform the subspace computation as follows:

$$\mathbf{R_{XX}}(f)\mathbf{V}(f) = \mathbf{R_{NN}}(f)\mathbf{V}(f)\mathbf{\Lambda}(f), \tag{3.10}$$

where $\mathbf{V}(f) = [\mathbf{v_1}(f)\ \mathbf{v_2}(f)\ \cdots\ \mathbf{v}_N(f)]$, $\mathbf{\Lambda}(f) = \text{ diag }\{\lambda_1(f), \lambda_2(f), \cdots, \lambda_N(f)\}$, $\lambda_i(f) \leq \lambda_j(f)$, for $i > j$, and $\mathbf{v}_i(f)$ is the eigenvector corresponding to eigenvalue $\lambda_i(f)$. It is well known that the largest M eigenvectors form the basis of the column space $R\{\mathbf{A}(f)\}$ of $\mathbf{A}(f)$, and the remaining $N - M$ eigenvectors form the basis of the orthogonal complement $R^{\perp}\{\mathbf{A}(f)\}$ of $R\{\mathbf{A}(f)\}$. The subspaces $R\{\mathbf{A}(f)\}$ and $R^{\perp}\{\mathbf{A}(f)\}$ are the signal subspace and noise subspace, respectively.

The ambient noise $\mathbf{n}(f)$ is almost omnidirectional and the correlation is small [31]. It is reasonable to assume that the noise covariance matrix is $\mathbf{R_{NN}}(f) = \sigma_f^2 \mathbf{I}_N$, where σ_f^2 is an unknown constant for frequency f. Without loss of generality, we assume $\sigma_f^2 = 1$ for all frequencies. Thus, the generalized eigenvalue decomposition becomes the standard eigenvalue decomposition

$$\mathbf{R_{XX}}(f)\mathbf{V}(f) = \mathbf{V}(f)\mathbf{\Lambda}(f). \tag{3.11}$$

For non-uniform linear arrays, the multiple signal classification (MUSIC) algorithm can be employed to estimate the DOAs. MUSIC algorithm computes the following pseudo-spectrum as a function of θ:

$$P_f(\theta) = \frac{\mathbf{a}_f^H(\theta)\mathbf{a}_f(\theta)}{\mathbf{a}_f^H(\theta)\mathbf{E}_N(f)\mathbf{E}_N^H(f)\mathbf{a}_f(\theta)}, \tag{3.12}$$

where $\mathbf{E}_N(f) = [\mathbf{v}_{M+1}(f) \ \cdots \ \mathbf{v}_N(f)]$, and $\mathbf{a}_f(\theta) = [e^{-j2\pi f d_1 \sin\theta/c}, \cdots, e^{-j2\pi f d_N \sin\theta/c}]^T$. The pseudo-spectrum is a measure of the closeness between an element of array manifold, which is the set of all array response vectors obtained as $\{\theta_m\}$ ranges over the entire parameter space, and signal subspace $R\{\mathbf{A}(f)\}$. In the absence of noise, it is infinite for elements of array manifold belonging to signal subspace $R\{\mathbf{A}(f)\}$. In the presence of noise, the M largest peaks in the pseudo-spectrum correspond to the M source directions. One drawback of the MUSIC algorithm is that it needs to compute the spectrum values for all directions, which results in huge computational burden. Additionally, the peak search algorithm further adds the computational cost.

Conversely, the estimation of signal parameters via rotational invariance techniques (ESPRIT) algorithm directly gives DOA estimates after obtaining the signal subspace, while it only applies to a uniform linear array. The ESPRIT algorithm is conducted as follows [32]:

(1) Choose the eigenvectors corresponding to the M largest eigenvalues, and form the matrix $\mathbf{G}(f) = [\mathbf{v}_1(f) \ \mathbf{v}_2(f) \ \cdots \ \mathbf{v}_M(f)]$, $\mathbf{G}_1(f) = [\mathbf{I}_{N-1} \ \mathbf{0}]\mathbf{G}(f)$, and $\mathbf{G}_2(f) =$

$[\mathbf{0}\ \mathbf{I}_{N-1}]\mathbf{G}(f)$, where $\mathbf{I}_{N-1}$ is the $N-1$ dimension identity matrix, and $\mathbf{0}$ is a $N-1$ dimension vector with all zero elements.

Therefore,

$$\begin{aligned}\mathbf{R_{XX}}(f)\mathbf{G}(f) &= \mathbf{G}(f)\mathbf{\Lambda}(f) &(3.13)\\ &= \mathbf{A}(f)\mathbf{R_{SS}}(f)\mathbf{A}^H(f)\mathbf{G}(f)+\mathbf{G}(f), &(3.14)\end{aligned}$$

where $\mathbf{\Lambda}(f)=\mathrm{diag}\{\lambda_1(f),\lambda_2(f),\cdots,\lambda_M(f)\}$. It follows that

$$\mathbf{G}(f)\mathbf{\Lambda}(f)-\mathbf{G}(f)=\mathbf{G}(f)\widetilde{\mathbf{\Lambda}}(f)=\mathbf{A}(f)\mathbf{R_{SS}}(f)\mathbf{A}^H(f)\mathbf{G}(f), \tag{3.15}$$

where $\widetilde{\mathbf{\Lambda}}(f)=\mathbf{\Lambda}(f)-\mathbf{I}$. Therefore,

$$\mathbf{G}(f)=\mathbf{A}(f)\mathbf{C}(f), \tag{3.16}$$

where $\mathbf{C}(f)=\mathbf{R_{SS}}(f)\mathbf{A}^H(f)\mathbf{G}(f)\widetilde{\mathbf{\Lambda}}^{-1}(f)$.

Let $\mathbf{A}_1(f)=[\mathbf{I}_{N-1}\ 0]\mathbf{A}(f)$, and $\mathbf{A}_2(f)=[0\ \mathbf{I}_{N-1}]\mathbf{A}(f)$. For a uniform linear array, it is clear that

$$\mathbf{A}_2(f)=\mathbf{A}_1(f)\mathbf{D}(f), \tag{3.17}$$

where $\mathbf{D}(f)=\mathrm{diag}\{e^{j2\pi fd\sin(\theta_1)/c},\cdots,e^{j2\pi fd\sin(\theta_M)/c}\}$, d is the inter-microphone spacing, and $d=|d_i-d_j|$, for $|i-j|=1$. Thus,

$$\mathbf{G}_2(f)=\mathbf{A}_2(f)\mathbf{C}(f)=\mathbf{A}_1(f)\mathbf{D}(f)\mathbf{C}(f)=\mathbf{G}_1(f)\mathbf{C}^{-1}(f)\mathbf{D}(f)\mathbf{C}(f)=\mathbf{G}_1(f)\mu(f), \tag{3.18}$$

where $\mu(f)=\mathbf{C}^{-1}(f)\mathbf{D}(f)\mathbf{C}(f)$. We get an $M\times M$ matrix

$$\mu(f)=(\mathbf{G}_1^H(f)\mathbf{G}_1(f))^{-1}\mathbf{G}_1^H(f)\mathbf{G}_2(f). \tag{3.19}$$

(2) The M eigenvalues $\{(\lambda_m(f))_{1\le m\le M}\}$ of $\mu(f)$ correspond to $\{(e^{j2\pi fd\sin(\theta_m)/c})_{1\le m\le M}\}$. Therefore, the estimated DOAs can be computed according to

$$\widetilde{\theta}_m(f)=\arcsin\{\mathrm{Im}\{\ln(\lambda_m(f))c/(2\pi fd)\}\}, \tag{3.20}$$

where $\arcsin\{\cdot\}$ is the inverse sine function, $\mathrm{Im}\{\cdot\}$ gives the imaginary part of a complex number, and $\ln(\cdot)$ is the natural logarithm operator.

After having multiple DOA estimates $\{(\widetilde{\theta}_m(f))_{1\leq m\leq M}\}$ at all frequencies, we will apply some rules to obtain final DOA estimates $\{(\widetilde{\theta}_m)_{1\leq m\leq M}\}$.

3.2.3 Final DOA Determination

At each frequency, we have the DOA estimates of the sources. However, because of the differences in signal power, noise power and thus SNRs at different frequency values, the estimated DOAs can vary a lot. Therefore, how to choose the frequencies with high SNRs and combine the estimates at these frequencies is a crucial issue. Since high SNRs ensure better DOA estimates, we try to use the DOA estimates from frequency components with high SNRs. In reality, only mixtures are given, and thus true SNRs are unknown.

In simulations, noise is assumed to be additive white Gaussian. Therefore, noise power is almost equally distributed over different frequencies, while signal power is different at different frequencies. Thus, the mixtures' SNRs at different frequencies are generally proportional to the signal power at corresponding frequencies and thus to the mixture power. The mixture power at different frequencies here is represented by the sums of squared amplitudes (SSAs) of the mixture spectrograms at corresponding frequencies. We choose the DOA estimates at the frequencies with high SSA values. However, the SSA values are attributed to multiple source signals' contributions in signal power. Therefore, the separate SNRs may be quite different and so are their DOA estimates. We use the average or the weighted average of the DOA estimates. For the weighted average, the weights are the normalized SSA values. In experiments, the noise is mainly at low frequencies and we choose relatively high frequencies in which the noise is generally much less. The same method for the simulations is then applied.

To summarize, we adopt the following rule.

(1) Use principle component analysis (PCA) to get M principle components of the mixtures $\mathbf{X}(p,f)$ at each frequency f. That is, we have $\overline{\mathbf{X}}(p,f) = \mathbf{G}^H(f)\mathbf{X}(p,f)$, for $p = 1, \cdots, P$.

(2) Choose Q frequencies $\{(f_q)_{1\le q\le Q}\}$ with the largest SSAs. The SSA at frequency f is defined as $SSA(f) = \sum_{p=1}^{P} \left\|\overline{\mathbf{X}}(p,f)\right\|_2^2$.

(3) The final estimate $\widetilde{\theta}_m$ for source m is obtained by averaging the DOA estimates at these frequencies $\widetilde{\theta}_m = \sum_{q=1}^{Q} \widetilde{\theta}_m(f_q)$, or using the weighted average of the DOA estimates $\widetilde{\theta}_m = \sum_{q=1}^{Q} \widetilde{\theta}_m(f_q) \frac{SSA(f_q)}{\sum_{q=1}^{Q} SSA(f_q)}$.

After obtaining the DOA estimates $\{(\widetilde{\theta}_m)_{1\le m\le M}\}$, we can calculate the estimated mixing matrix $\widetilde{\mathbf{A}}(f) = [\mathbf{a}(\widetilde{\theta}_1)\ \mathbf{a}(\widetilde{\theta}_2)\ \cdots\ \mathbf{a}(\widetilde{\theta}_M)]$. The demixing matrix $\widetilde{\mathbf{W}}(f)$ for each frequency f can be obtained by using the least square estimates with the constraint $\widetilde{\mathbf{W}}(f)\widetilde{\mathbf{A}}(f) = \mathbf{I}$. That is, $\widetilde{\mathbf{W}}(f)$ is the pseudo-inverse of $\widetilde{\mathbf{A}}(f)$. Then, use $\widetilde{\mathbf{S}}(p,f) = \widetilde{\mathbf{W}}(f)\mathbf{X}(p,f)$ for all frequencies. Using the inverse STFT, we can recover the time domain source signals $\widetilde{\mathbf{s}}(t)$.

3.3 Related Issues and Solutions

It is noted that we use the subspace methods at each frequency, compute the sample covariance matrix to approximate the true covariance matrix, and thus assume that the signal at each frequency is wide sense stationary. In fact, whether the signal at one particular frequency is stationary during specific time intervals and how stationary it is affect the DOA estimation performance of the subspace methods.

3.3.1 Source Number Estimation

In the previous section, the number of sources is assumed to be known beforehand and smaller than the number of microphones. In practice, the source number can be determined by analyzing the eigenvalues $\{(\lambda_i(f))_{1\leq i\leq N}\}$ of the covariance matrix of the mixtures at frequency f. That is, the number of dominant eigenvalues implies the number of sources. Therefore, a subjective threshold on the eigenvalues of the covariance matrix can be set to estimate the source number.

Another approach is based on the information theoretical criteria. Akaike information criterion (AIC) [33] and minimum description length (MDL) [34, 35] are two common criteria to estimate the source number. They intend to minimize a measure consisting of the log-likelihood of the maximum likelihood estimator of the parameters of the model and a bias correction term. The main difference lies in the bias correction term. To be more specific, the AIC chooses the source number estimate $\widehat{M}$ minimizing:

$$-2\log\left(\frac{\prod_{i=\widehat{M}+1}^{N}\lambda_i(f)^{1/(N-\widehat{M})}}{\frac{1}{N-\widehat{M}}\sum_{i=\widehat{M}+1}^{N}\lambda_i(f)}\right)^{(N-\widehat{M})P}+2\widehat{M}(2N-\widehat{M}), \tag{3.21}$$

where $0\leq\widehat{M}\leq N-1$. The MDL selects the $\widehat{M}$ minimizing:

$$-\log\left(\frac{\prod_{i=\widehat{M}+1}^{N}\lambda_i(f)^{1/(N-\widehat{M})}}{\frac{1}{N-\widehat{M}}\sum_{i=\widehat{M}+1}^{N}\lambda_i(f)}\right)^{(N-\widehat{M})P}+0.5\widehat{M}(2N-\widehat{M})\log P. \tag{3.22}$$

Theoretically, the AIC is more likely to give an overestimation value, while the MDL's estimation is unbiased [36].

3.3.2 Frequency Bin Selection

It is known in the array signal processing literature that, for a broadband signal, its high frequency components prefer small array spacing, while its low frequency

parts prefer large spacing. In reality, a given microphone array is fixed and signals of interest can be different. In [37], the authors propose using microphones with different spacing to handle different frequency ranges respectively. That is, considering that we need multiple microphones to perform localization, we may select only a subset of the microphones to perform the localization for lower frequency signals, as long as the source number is less than the number of chosen microphones. Therefore, a microphone array can handle a wider range of signals.

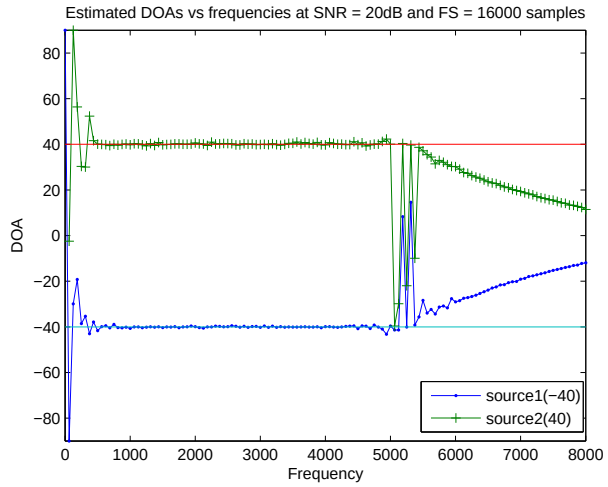

Figure 3.2: DOA estimate versus frequency for two sources at -40 and 40 degrees.

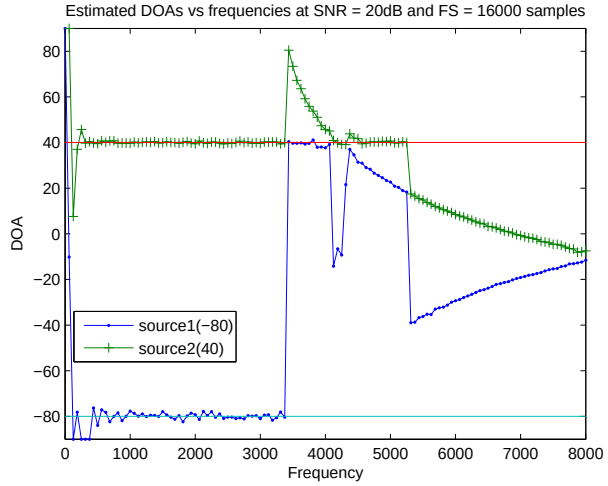

Figure 3.3: DOA estimate versus frequency for two sources at -80 and 40 degrees.

A microphone array samples signals in the space domain. Similar to the aliasing problem for sampling in the time domain, a microphone array also experiences a spatial aliasing problem. In the time domain, the well-known Nyquist sampling theory tells that to recover a signal with the highest frequency f_{max}, the sampling rate is at least $2f_{max}$. In the spatial sampling, it requires that half of the minimum wavelength of a wideband signal should be larger than the interval of the array upon which it impinges. To be more specific, for a microphone spacing d, the maximum frequency it can capture accurately is $c/(2d)$, where c is the velocity of sound in the medium. In our problem, the phase delay between two microphones should be smaller than π in modulus, i.e., $|2\pi f d sin(\theta)/c| \leq \pi$. For example, when $d = 0.05$ m, $c = 340$ m/s, $\theta_1 = -40$ degree, and $\theta_2 = 40$ degree, the spatial aliasing occurs at $c/2/sin(40\pi/180) = 5289.5$Hz. Figure 3.2 shows how the estimated DOA changes with frequency. At around 5000 Hz, the DOA estimate becomes drastically inaccurate. When $\theta_1 = -80$ degree, $\theta_2 = 40$ degree, and other parameters remain the same, the spatial aliasing occurs at $c/(2sin(80\pi/180)) = 3452.5$ Hz. Figure 3.3 shows that the tipping point where the estimate becomes much worse is at around 3400 Hz. This suggests that we only focus on the frequency range where no spatial aliasing occurs.

On the other hand, if the frequency of a signal is too low and thus its wavelength is too long, the array can only capture a very tiny amount of the phase change of the signal. From Figures 3.2 and 3.3, it is clear that the DOA estimate is significantly worse at low frequencies than at higher frequencies. Therefore, a lower frequency threshold is also set. Although audio signals are naturally broadband, we can only consider some specific frequencies, at which the algorithm can estimate the DOAs more accurately.

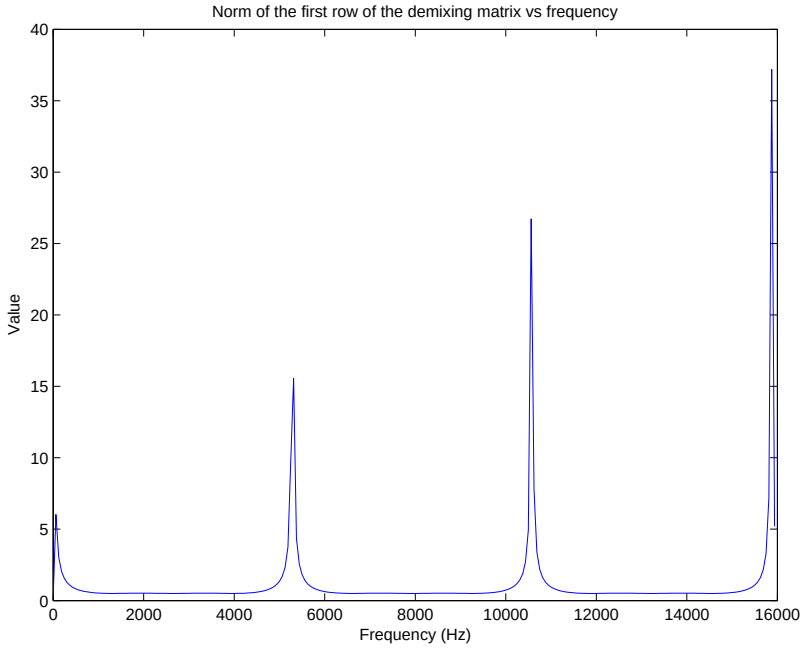

Figure 3.4: Norm of the first row of $\widetilde{\mathbf{W}}(f)$ versus frequency f.

3.3.3 Artifact Filtering

It is noted that for estimated DOAs, mixing matrix $\mathbf{A}(f)$'s columns are linearly dependent at certain harmonic frequencies so that $\widetilde{\mathbf{W}}(f)$ becomes extremely large at these frequencies. For example, Figure 3.4 shows one example of how the second norm of the first row of the estimated demixing matrix $\widetilde{\mathbf{W}}(f)$ changes with frequency using the estimated DOAs. It is clear that the large values are distributed at harmonic frequencies. Consequently, recovered signals include burbling artifacts, which are known as "musical notes" in the literature [38]. An easy way to eliminate these artifacts is to use certain filters to eliminate the recovered signals at these frequencies.

3.3.4 Different Ways of Mixture Generation

The subspace methods utilize the phase differences among the mixtures collected by different microphones. Namely, the success of our algorithm largely depends on the accuracy of the phase difference measurements among array signals. In practice, we

only have discrete time signals and correspondingly measured time delays are only approximated by an integer number of sampling intervals. Therefore, sampling rate plays an important role. For our algorithm to work, it should satisfy the condition:

$$d\sin\theta/c \geq \frac{1}{F_s}. \tag{3.23}$$

For small angles and low sampling rates, the algorithm may fail if time domain mixtures are used, due to the fact that the delay may be less than a sampling interval and there will be no delay and phase change information in the collected mixtures at different microphones. In other words, sampling results in rounding errors in the measured phase changes and time delays, and generating biases in the DOA estimates. The round error in the time delay between two adjacent microphones equals $(d\sin\theta/c - \frac{N}{F_s})$ second(s), where $N = \text{floor}(d\sin\theta F_s/c)$, and $\text{floor}(a)$ returns the nearest integer no larger than a.

In simulations, we try two different mixing approaches to reduce or eliminate the effect of sampling. First is to use source signals with as high sample rates as possible. Second is to use mixtures in the frequency domain so that the phase information is free from the sampling effect. That is, the mixture is generated by the formula $\mathbf{X}(p,f) = \mathbf{A}(f)\mathbf{S}(p,f) + \mathbf{N}(p,f)$, and the SNRs are set in the time domain. For frequency domain mixtures, the phase differences among different microphones are totally preserved. While this may not reflect the natural experimental procedure, this helps us focus on other aspects of the algorithm without the finite sampling rate effect. Figure 3.5 shows the difference in obtaining a time domain mixture and a frequency domain mixture.

3.3.5 Relation with Beamforming and Spatial Filtering

We use the subspace methods to estimate the DOAs of sources and separate the source signals using the DOA estimates. This is essentially related to spatial filtering, or beamforming in the array signal processing literature. It shows that in the simulations

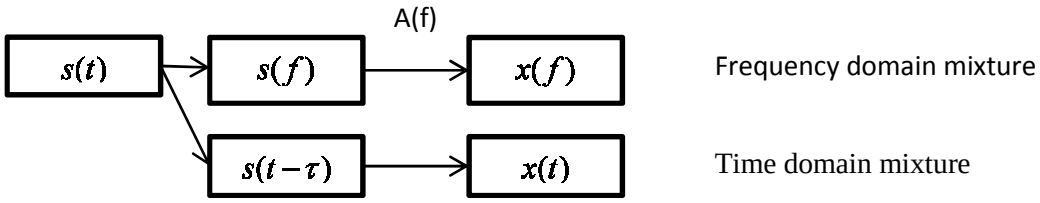

Figure 3.5: Two different kinds of mixtures.

and experiments, even if the estimated DOAs which are deviated significantly from the true ones are used, and thus the separation performance becomes worse and burbling artifacts are significant, the original sounds can still be audible clearly from the recovered files. Especially, when the sources are widely separated, as long as the estimates can roughly reflect the spatial locations of the sources, the sounds can be heard without too much performance loss.

3.3.6 Performance Measures

The performance measures used for evaluation include the mean squared error (MSE) of DOA or coordinate estimates for localization and the signal-to-distortion ratio (SDR), the signal-to-interferences ratio (SIR), and the signal-to-artifacts ratio (SAR) for separation, which are firstly introduced in [38]. The MSE of DOA estimate $\theta_m(f)$ for source m at frequency f is computed as

$$\mathrm{MSE}_{\theta_m(f)} = \frac{\sum_i (\tilde{\theta}_{m,i}(f) - \theta_m)^2}{I}, \tag{3.24}$$

where I is the number of Monte Carlo runs. The MSE of DOA estimate θ_m is computed as

$$\mathrm{MSE}_{\theta_m} = \frac{\sum_i (\tilde{\theta}_{m,i} - \theta_m)^2}{I}, \tag{3.25}$$

The MSE of source coordinate estimate $\mathbf{v}_m$ for source m is computed as

$$\mathrm{MSE}_{\mathbf{v}_m} = \frac{\sum_i ||\tilde{\mathbf{v}}_{m,i} - \mathbf{v}_m||^2}{I}. \tag{3.26}$$

where $\mathbf{v}_m$ and $\tilde{\mathbf{v}}_{m,i}$ are $D \times 1$ vectors, and D is the dimension of the coordinate system. In our problem, we consider the two-dimension system, i.e., $D = 2$.

For separation, it is assumed that the recovered source signal can be decomposed through orthogonal projections as

$$\hat{\mathbf{s}}_m = \mathbf{s}_{\text{target}} + \mathbf{e}_{\text{interf}} + \mathbf{e}_{\text{noise}} + \mathbf{e}_{\text{artif}}, \tag{3.27}$$

where $\mathbf{s}_{\text{target}}$ is a modified version of $\mathbf{s}_m$ with an allowed distortion, $\mathbf{e}_{\text{interf}}$, $\mathbf{e}_{\text{noise}}$, and $\mathbf{e}_{\text{artif}}$ are respectively the interferences, noise, and artifacts terms. $\hat{\mathbf{s}}_m$, $\mathbf{s}_{\text{target}}$, $\mathbf{e}_{\text{interf}}$, $\mathbf{e}_{\text{noise}}$, and $\mathbf{e}_{\text{artif}}$ are $L \times 1$ vectors, and L is the source signal length measured in samples.

To be more specific, let $\prod\{\mathbf{z}_1, \mathbf{z}_2, \cdots, \mathbf{z}_j\}$ represent the orthogonal projector onto the subspace spanned by the vectors $\mathbf{z}_1, \mathbf{z}_2, \cdots, \mathbf{z}_j$. The projector is a $J \times J$ matrix, where J is the length of these vectors. The decomposition includes three projectors:

$$P_{\mathbf{s}_m} := \prod\{\mathbf{s}_m\}, \tag{3.28}$$

$$P_{\mathbf{s}} := \prod\{(\mathbf{s}_m)_{1 \le m \le M}\}, \tag{3.29}$$

and

$$P_{\mathbf{s},\mathbf{n}} := \prod\{(\mathbf{s}_m)_{1 \le m \le M}, (\mathbf{n}_n)_{1 \le n \le N}\}. \tag{3.30}$$

where $\mathbf{s}_m$ and $\mathbf{n}_m$ are $L \times 1$ vectors. The four terms are written as follows:

$$\mathbf{s}_{\text{target}} := P_{\mathbf{s}_m} \hat{\mathbf{s}}_m, \tag{3.31}$$

$$\mathbf{s}_{\text{interf}} := P_{\mathbf{s}} \hat{\mathbf{s}}_m - P_{\mathbf{s}_m} \hat{\mathbf{s}}_m, \tag{3.32}$$

$$\mathbf{s}_{\text{noise}} := P_{\mathbf{s},\mathbf{n}} \hat{\mathbf{s}}_m - P_{\mathbf{s}} \hat{\mathbf{s}}_m, \tag{3.33}$$

and

$$\mathbf{s}_{\text{artif}} := \hat{\mathbf{s}}_m - P_{\mathbf{s},\mathbf{n}}\hat{\mathbf{s}}_m. \tag{3.34}$$

The SDR is defined as

$$\text{SDR} = 10\ \log_{10}\frac{||\mathbf{s}_{\text{target}}||^2}{||\mathbf{e}_{\text{interf}} + \mathbf{e}_{\text{noise}} + \mathbf{e}_{\text{artif}}||^2}. \tag{3.35}$$

The SIR is defined as

$$\text{SIR} = 10\ \log_{10}\frac{||\mathbf{s}_{\text{target}}||^2}{||\mathbf{e}_{\text{interf}}||^2}. \tag{3.36}$$

The SAR is defined as

$$\text{SAR} = 10\ \log_{10}\frac{||\mathbf{s}_{\text{target}} + \mathbf{e}_{\text{interf}} + \mathbf{e}_{\text{noise}}||^2}{||\mathbf{e}_{\text{artif}}||^2}. \tag{3.37}$$

The underlying assumption is that the ground truth source signals and noise are known. The existing computer algorithms for recovered signal decomposition and SDR, SAR, and SIR computation can be found in [39].

3.3.7 Source Coordinate Estimation using Multiple Arrays

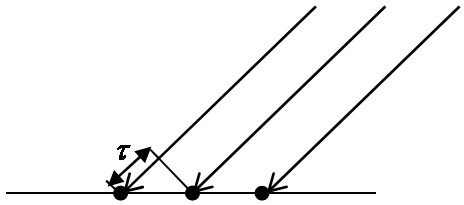

Figure 3.6: Relative delay mixing.

One array can estimate the DOAs of sources, and multiple arrays can together determine the coordinates of the sources. Once we have the DOA estimates for the same source at multiple arrays, its coordinates can be computed using triangulation techniques combined with the knowledge about the coordinates of the arrays. In our localization scheme, we assume that different sources have different source angles with respect to one array. The underlying assumption here is that the sources are placed

in a far field area of the microphone arrays. Therefore, for the microphones on one array, their angles with respect to the same source are the same, which is represented by the angle between the source and the array center. This is shown in Figure 3.6. The relative delay between the signals from the same source collected by two adjacent microphones is shown as τ. We can use this relative delay to generate mixtures. We

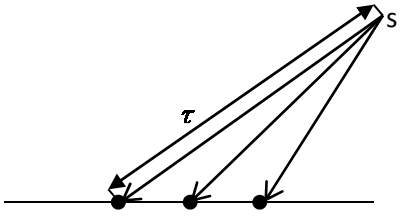

Figure 3.7: Absolute delay mixing.

can also use absolute delays shown in Figure 3.7 to generate mixtures. As to the absolute delays, the angles between the microphones on the same array and the same source are different. These two scenarios are similar when the sources are far away from the microphone arrays.

We compare our method with the algorithm proposed in [1] referred to as "Nion's method" in the following. Both algorithms are tested using four different kinds of mixtures. That is, mixing in the frequency domain using relative delays, mixing in the frequency domain using absolute delays, mixing in the time domain using relative delays, and mixing in the time domain using absolute delays.

The comparable algorithm uses an alternating least square (ALS) algorithm to recover the source signals and mixing matrices, while enforcing the constraint that the mixing matrices at different frequencies have the Vandermonde structure. The estimated mixing matrices are modified versions of the true mixing matrices. Selecting a reference sensor helps eliminate the ambiguities. The TDOAs are used to localize the sources.

To be more specific, M sources and N microphones can be placed arbitrarily. The microphones are not necessarily on an array as required for our method. Similar to our

formulation, the received mixture at microphone n is represented in Equation (3.1). Moreover, it is not necessarily a far field, and the DOAs of the same source are not necessarily equal for the multiple microphones on the same array.

After performing K point STFT,

$$X_n(p, f_k) = \sum_{m=1}^{M} a_{nm} S_m(p, f_k) e^{-j2\pi f_k \tau_{nm}} + N_n(p, f_k), \tag{3.38}$$

where $f_k = F_s(k-1)/K$ represents the frequency value, for $k = 1, \cdots, F$, and $F = \text{floor}(K/2) + 1$. f is the shorthand notation for f_k in the following. The noise part is ignored in the theoretical analysis for the sake of simplicity. Therefore,

$$\mathbf{X}(f) = \mathbf{H}(f)\mathbf{S}(f), \tag{3.39}$$

where $[\mathbf{X}(f)]_{n,p} = X_n(p, f)$, $[\mathbf{S}(f)]_{m,p} = S_m(p, f)$, $w = e^{-j2\pi}$, and $[\mathbf{H}(f)]_{m,n} = a_{nm} w^{f\tau_{nm}}$.

Define $H_{n,m,f} = [\mathbf{H}(f)]_{n,m}$, $\mathbf{h}_{nm} = H_{n,m,1:F} = [a_{nm} w^{f_1 \tau_{nm}}, \cdots, a_{nm} w^{f_F \tau_{nm}}]^T$ has a Vandermonde structure. Namely, $\mathbf{h}_{nm} = a_{nm}[b^0, b^1, \cdots, b^F]^T$, where $b = w^{\tau_{nm} F_s/K}$. Then, $X \in C^{F \times N \times P}$ and $S_n \in C^{F \times F \times P}$, which are defined by $X_{f,n,p} = X_n(p, f)$ and $[S_m]_{:,:,p} = \text{diag}([S_m(p, 1), S_m(p, 2), \cdots, S_m(p, F)])$, respectively. Let $\mathbf{H}_m \in C^{F \times N}$ be the channel Vandermonde matrix for source m, which is defined as $[\mathbf{H}_m]_{:,n} = \mathbf{h}_{nm}$, where $\mathbf{H}_m$ is the part of H related to source m. Therefore,

$$X = \sum_{m=1}^{M} \mathbf{S}_m \bullet_2 \mathbf{H}_m^T. \tag{3.40}$$

where $\bullet_2$ is the tensor product operator. Figure 3.8 shows the tensor representation of Equation (3.40). Based on the received data $\mathbf{X}(f_k)$, for $k = 1, \cdots, F$, the ALS algorithm with the Vandermonde structure enforcement on $\mathbf{h}_{nm}$ is implemented to recover the $\mathbf{H}(f)$ and $\mathbf{S}(f)$ alternatively at each frequency. Due to the ambiguities inherent in the algorithm, it only recovers a modified version of $\mathbf{H}(f)$. That is, $\tilde{\mathbf{h}}_{nm} = [\tilde{a}_{nm} w^{f_1 \tilde{\tau}_{nm}}, \cdots, \tilde{a}_{nm} w^{f_F \tilde{\tau}_{nm}}]$. Therefore, a reference microphone m_R is chosen to eliminate the ambiguities and the TDOAs are obtained: $\overline{\tau}_{nm} = \tilde{\tau}_{nm} - \tilde{\tau}_{nm_R} =$

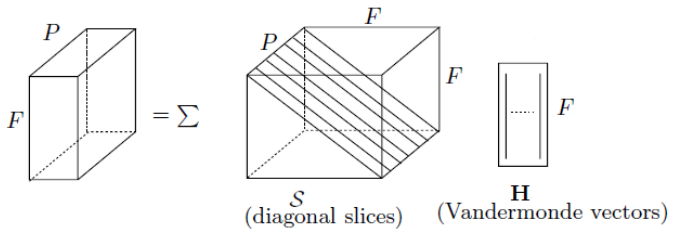

Figure 3.8: The tensor representation of the problem [1].

$\tau_{nm} - \tau_{nm_R}$. After having the multiple TDOAs, the sources are localized by solving a constrained optimization problem. A drawback of Nion's method is that it does not guarantee to converge. Its separation and localization results heavily depend on the initialization step. It is also time consuming.

CHAPTER 4

SIMULATIONS AND EXPERIMENTS FOR OUTDOOR ENVIRONMENTS

In this section, we firstly use MATLAB simulations to show the performance of the proposed algorithm. Then, we use experiments to show its effectiveness in real world environments. We mainly use uniform linear arrays and the ESPRIT method, given that the ESPRIT can directly give DOA estimates.

4.1 Simulations

4.1.1 Simulation Setup

In the simulations, there are $N = 4$ microphones uniformly and linearly distributed with spacing $d = 0.05$ m. $M = 2$ sources are located at directions $\theta_1 = 40$ and $\theta_2 = -40$ degrees, respectively. Source signals include music and speeches. They are normalized into signals with zero mean and unit variance. The velocity of sound in the air is $c = 340$ m/s. The sampling rate is 16 kHz. The noise is set to be zero mean additive white Gaussian noise (AWGN) with variance σ^2 across microphones. It is noted that for audio signals, the power at different frequencies are different, while the power of white noise at different frequencies are ideally equal. The signal-to-noise ratio is set to be $10\log_{10}(M/\sigma^2)$. We only consider the frequency range without spatial aliasing. That is, in our simulations, $f \leq c/(2d)$. We use 10000 Monte Carlo runs for each SNR. Additionally, in all simulations, due to the inability of a microphone array to capture low frequency signals, we set a lower frequency threshold to be 1 kHz. The parameter setting in simulations is summarized in Table 4.1.

Table 4.1: Parameter setting in simulations.

Mixture characteristics	Parameters to be specified
Number of sources M	2
Source categories	Speech & music
Source length	4 seconds
Source angles	+/- 40°
Noise type	AWGN (sensor noise)
Number of microphones N	4
Array spacing d	0.05 m
Sampling rate F_s	16 kHz
Mixture type	Pure delay mixture
Mixture domain	Frequency domain
Frame length	256
Frame shift	256
FFT window	Rectangular
Chosen frequency percentage	30%
Monte Carlo runs	10000

4.1.2 Source Spectrogram

The diverse time-frequency characteristics of audio signals can be illustrated by their spectrograms, which are the signal amplitude values as a function of time-frequency. Figure 4.1 shows the spectrograms of four sources. Source1 and Source2 are male and female speeches, respectively. Source3 and Source4 correspond to trumpet and piano music. They show typical time-frequency characteristics for each category. That is, speeches generally cross a wide spectrum and short time duration, while music consists of harmonic frequencies and is more continuous in time.

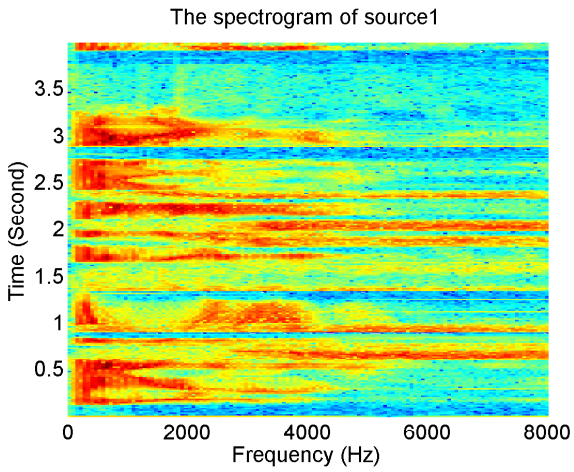

(a) Source1 (Male speech)

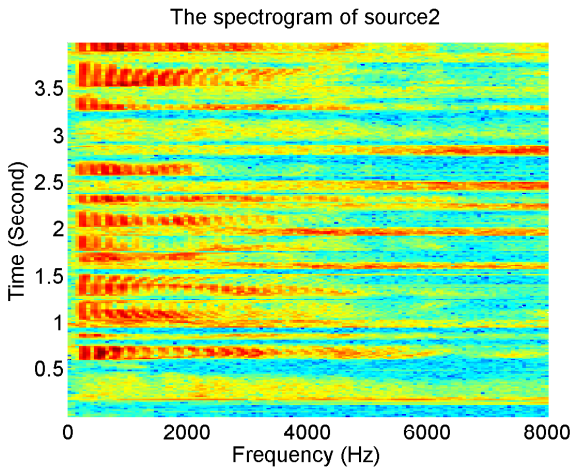

(b) Source2 (Female speech)

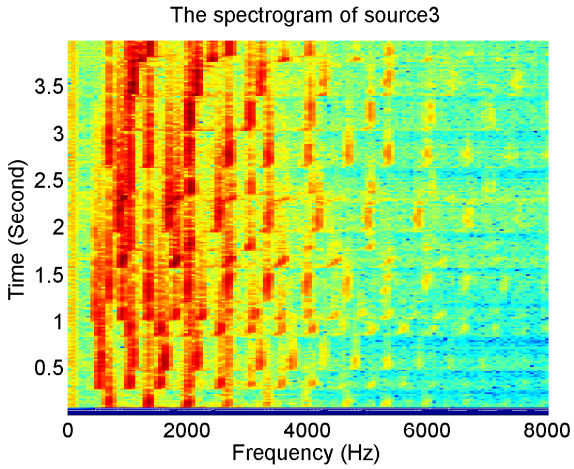

(c) Source3 (Trumpet music)

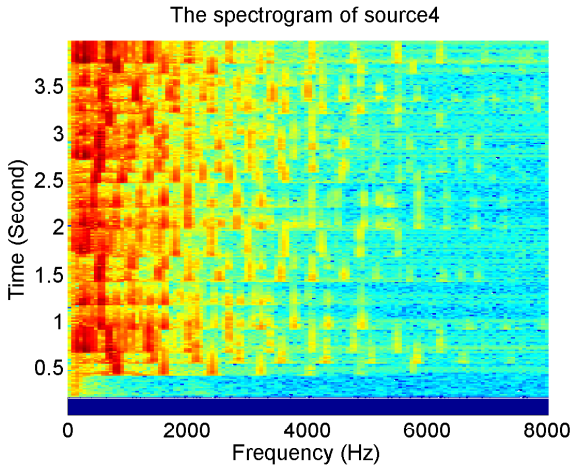

(d) Source4 (Piano music)

Figure 4.1: The spectrograms of different sources.

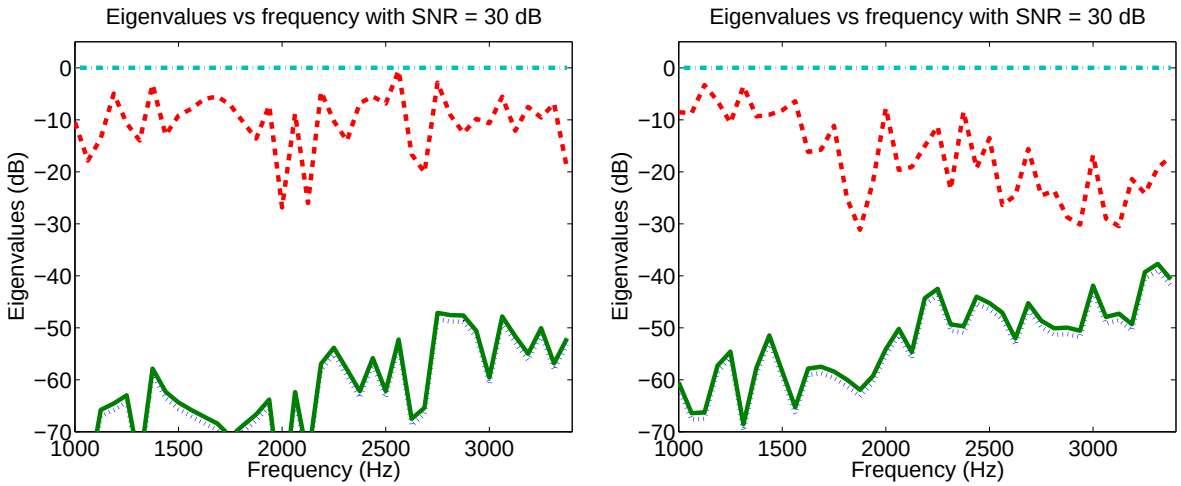

(a) Mixture of Source1 and Source3

(b) Mixture of Source2 and Source4

Figure 4.2: Normalized eigenvalues versus frequency for different source combinations with SNR = 30 dB.

4.1.3 Source Number Estimation

Eigenvalue based Method

Figure 4.2 shows the normalized eigenvalues of the covariance matrix at different frequencies for different source combinations at SNR = 30 dB. The plots are obtained by averaging the results over total 10000 runs. It is clear that for different sources, the whole trend of how eigenvalues change with frequency is different. With SNR = 30 dB, the first two eigenvalues are much larger than the rest eigenvalues for most of the frequencies. It is relatively easy to set a subjective threshold to decide the source number. That is, when the signal power is dominant in the mixture, using eigenvalue analysis to estimate source number is suitable.

Figure 4.3 shows the results for SNR = 10 dB. It is shown that for the mixture of Soure1 and Source3, at almost all frequencies, the two largest eigenvalues are significantly larger than the remaining two smaller eigenvalues. Therefore, the number of sources can be estimated accurately. For the mixture of Source2 and Source4, at frequencies from 1000 Hz to around 2000 Hz, the two largest eigenvalues can be

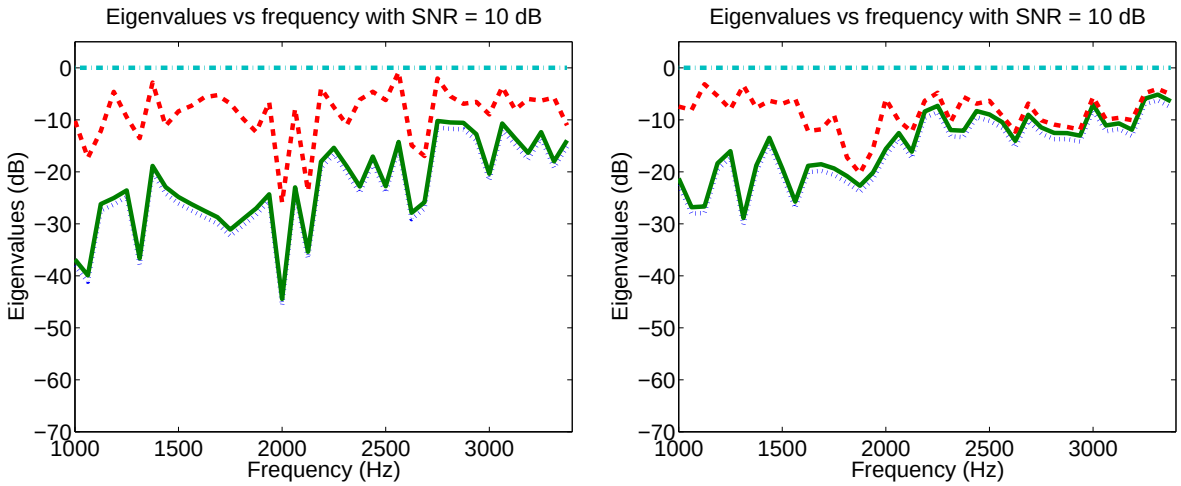

(a) Mixture of Source1 and Source3

(b) Mixture of Source2 and Source4

Figure 4.3: Normalized eigenvalues versus frequency for different source combinations with SNR = 10 dB.

easily distinguished from the rest. The two smaller eigenvalues are very close to the second largest eigenvalues at higher frequencies, which introduces ambiguities in the estimation of the source number. Intuitively, at lower SNRs, it will become more difficult to estimate the number of sources accurately by setting a threshold. Moreover, from Figure 4.3, we can learn that the differences in the patterns of how the eigenvalues change with frequency are closely related to the characteristics of sources.

Information Theoretical Criteria

Information theoretical criteria include Akaike information criterion (AIC) and minimum description length (MDL). Figures 4.4 and 4.5 show the percentage of correct source number estimates in total 10000 runs using AIC and MDL at SNR = 30 dB and 10 dB, respectively.

They indicate that higher SNRs bring a better source number estimation performance. At low SNRs, like 10 dB, source number estimation can be very different at different frequencies because of the difference of power distribution across frequency. For example, in Figures 4.5(c) and 4.5(d), the source number estimation accuracy at

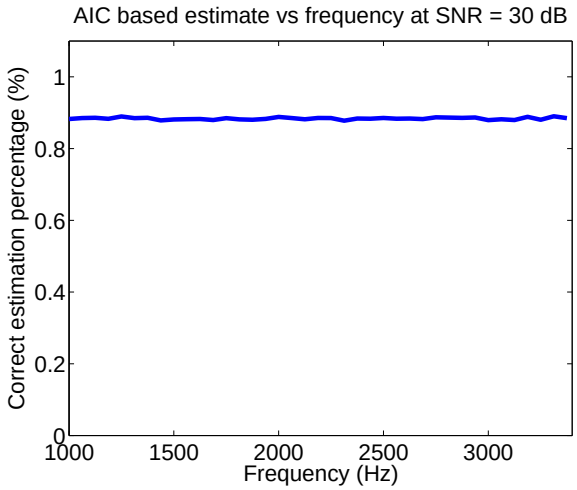

(a) Mixture of Source1 and Source3 using AIC

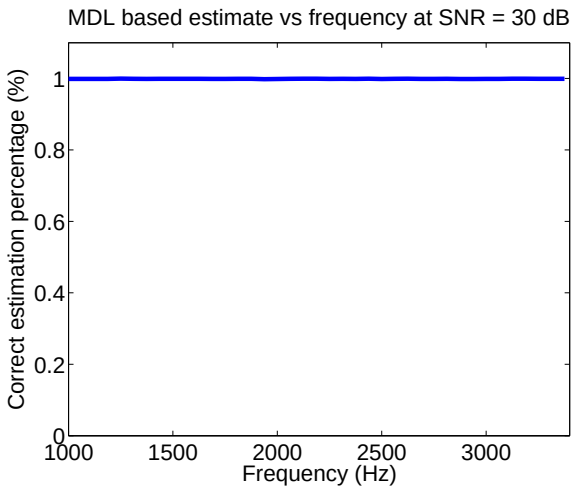

(b) Mixture of Source1 and Source3 using MDL

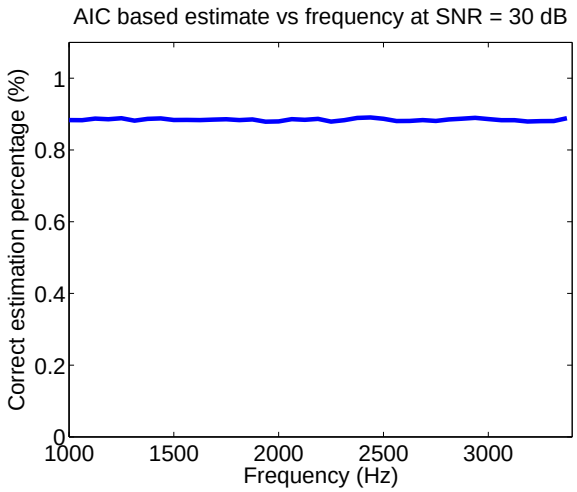

(c) Mixture of Source2 and Source4 using AIC

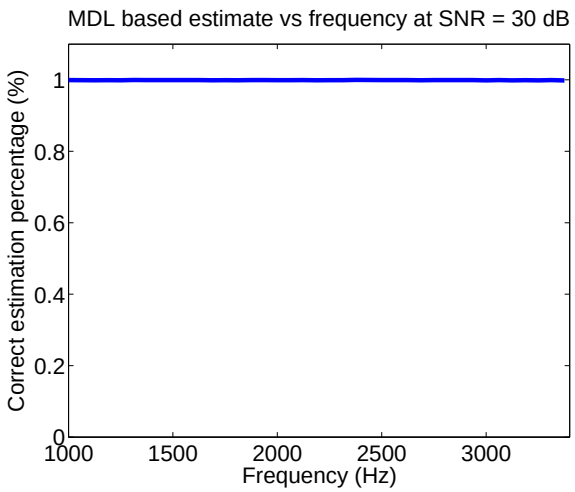

(d) Mixture of Source2 and Source4 using MDL

Figure 4.4: Correct estimation percentage versus frequency for different source combinations with SNR = 30 dB using AIC and MDL.

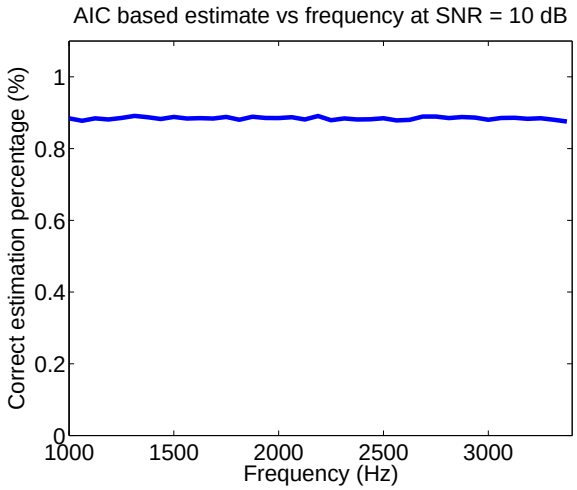

(a) Mixture of Source1 and Source3 using AIC

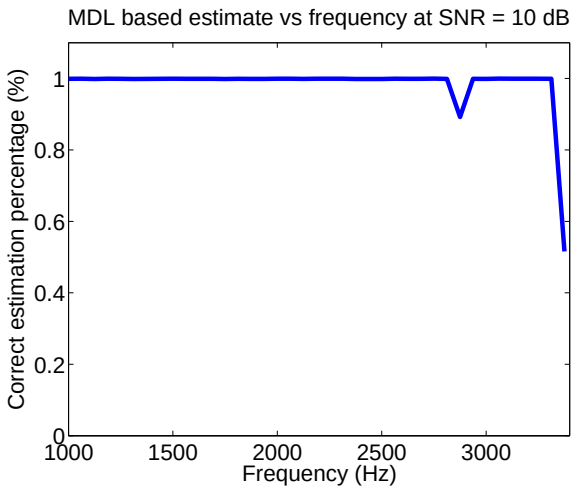

(b) Mixture of Source1 and Source3 using MDL

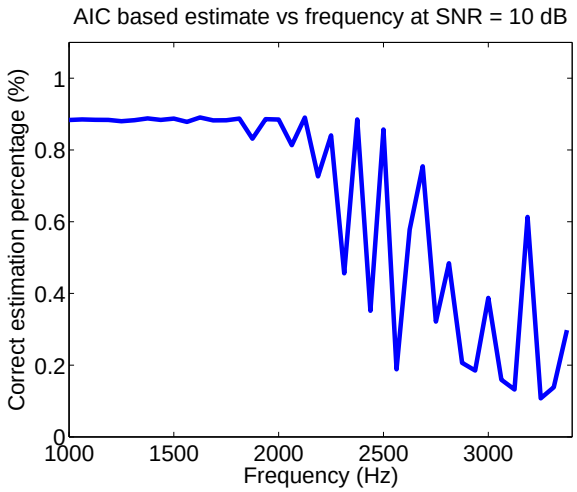

(c) Mixture of Source2 and Source4 using AIC

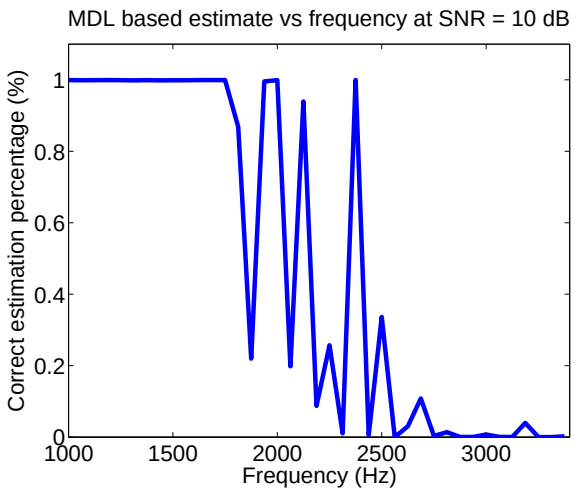

(d) Mixture of Source2 and Source4 using MDL

Figure 4.5: Correct estimation percentage versus frequency for different source combinations with SNR = 10 dB using AIC and MDL.

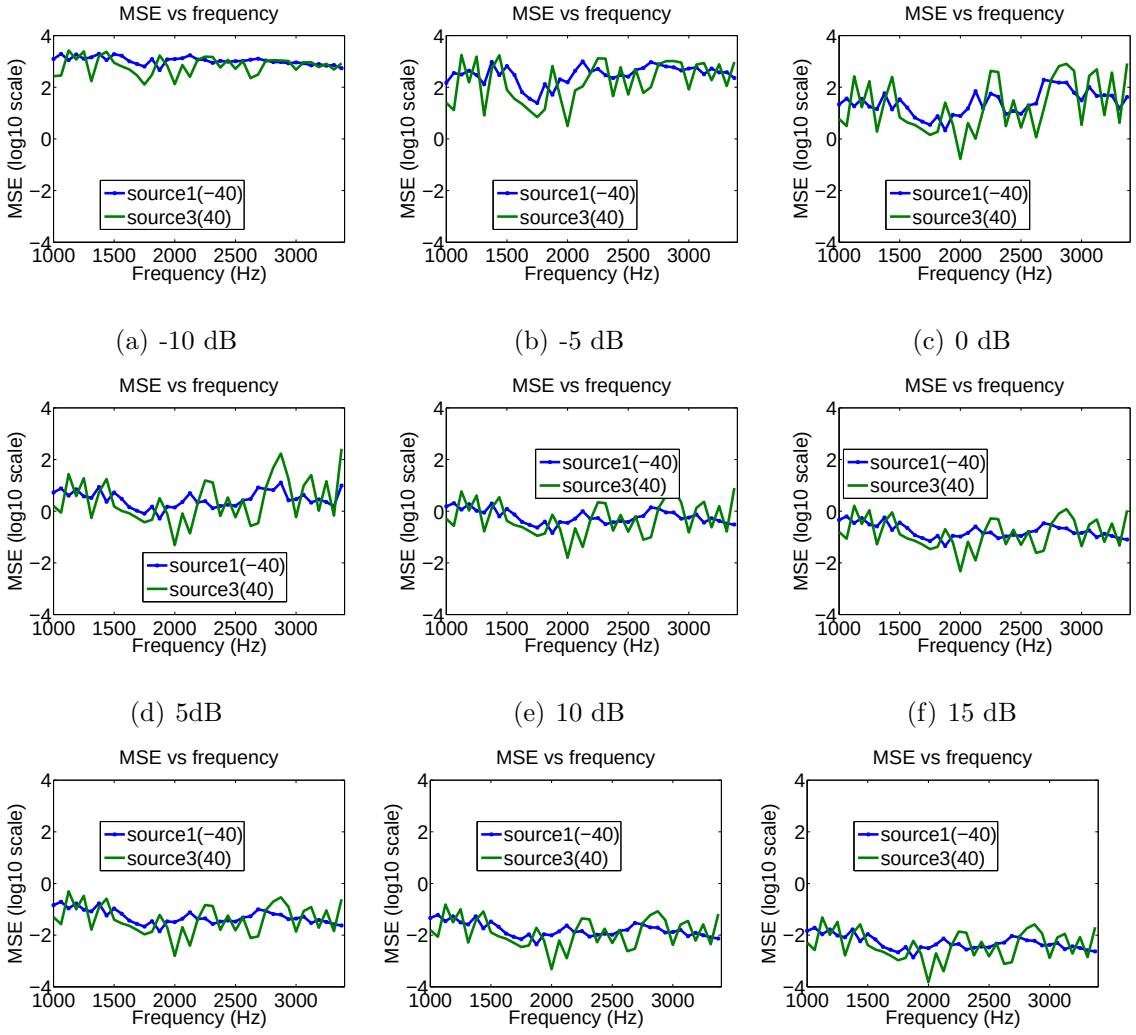

(a) -10 dB (b) -5 dB (c) 0 dB

(d) 5dB (e) 10 dB (f) 15 dB

(g) 20 dB (h) 25 dB (i) 30 dB

Figure 4.6: MSE versus frequency at different SNRs using Source1 and Source3.

certain frequencies larger than 2000 Hz deteriorates a lot. This is because there is much less power distributed above 2 kHz for Source2 and Source4, compared to the power distributed below 2 kHz, which is obvious from their spectrograms. Therefore, for an accurate source number estimation, it's desirable to have some knowledge about how the power of source signals is distributed across frequency.

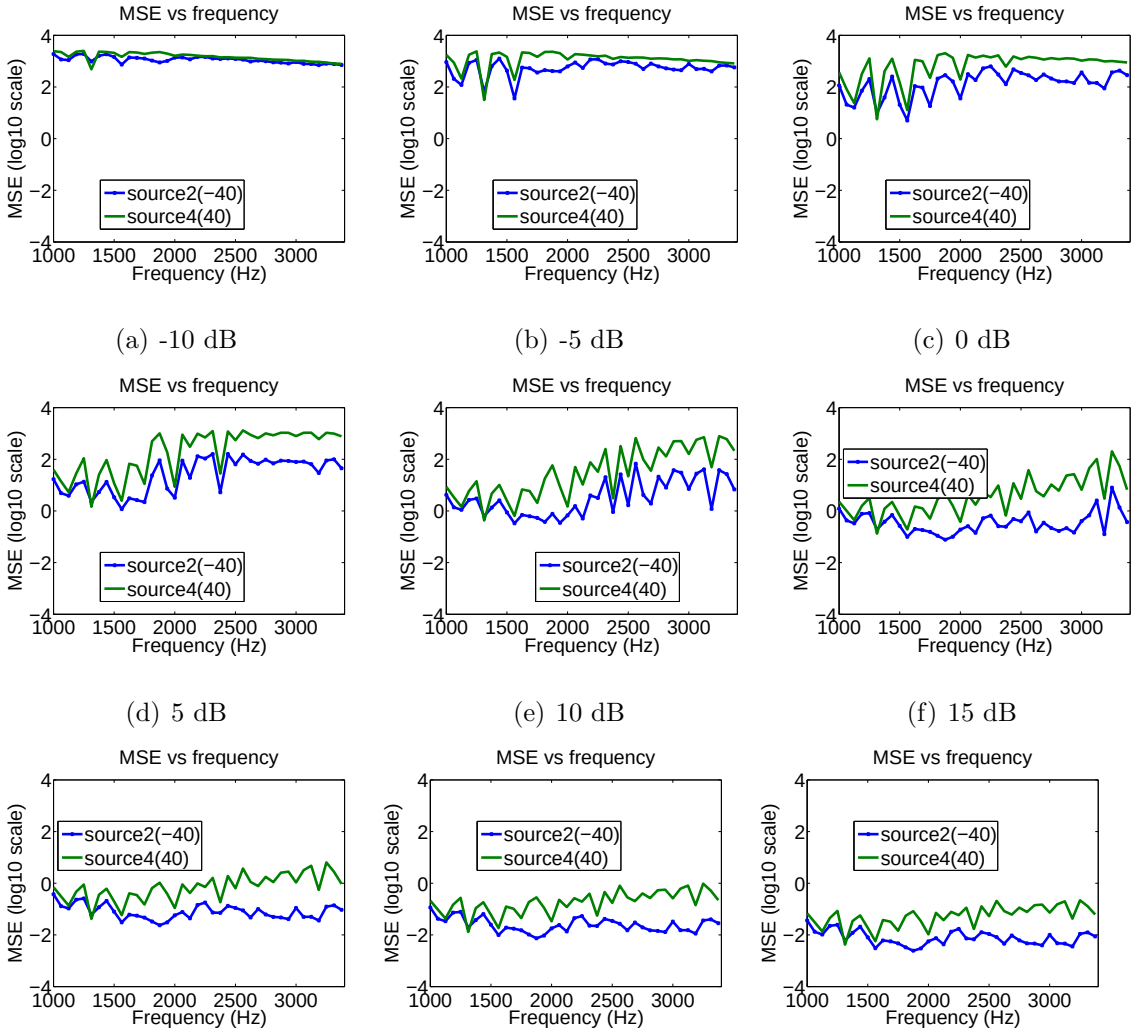

(a) -10 dB (b) -5 dB (c) 0 dB

(d) 5 dB (e) 10 dB (f) 15 dB

(g) 20 dB (h) 25 dB (i) 30 dB

Figure 4.7: MSE versus frequency at different SNRs using Source2 and Source4.

4.1.4 $\theta_m(f)$ Estimation and Associated Separation

$\theta_m(f)$ Estimation Performance

Figures 4.6 and 4.7 show the MSE versus frequency at different SNRs using the mixture of Source1 and Source3, and using the mixture of Source2 and Source4, respectively. It is obvious that with higher SNRs, the MSE performance is much better. For different source files, the patterns of MSE versus frequency curves are very different. This is likely to be related to the SNR difference of different signals at different frequencies and at different time locations. In other words, it is because of the differences of different source files in time-frequency characteristics.

Separation Performance

Figures 4.8, 4.9, 4.10, 4.11, 4.12, and 4.13 show the average SDR, SAR, and SIR versus frequency at different SNRs for different source combinations. Similarly, higher SNRs bring a better separation performance. Among these three measures, the SDR is most frequently used, due to the fact that it is the ratio of the power of the desired part of a recovered signal to the power of the undesired part.

It shows that at low SNRs, the SDR, SAR, and SIR values are extremely small, which indicates inaccurate DOA estimates and correspondingly an enormous amount of noise, artifacts, and interferences. As the SNR increases, the DOA estimates become more accurate, and thus the separation performance is better. Moreover, the SDR and SAR curves become more similar as the SNR increases. This is because the noise term diminishes with a higher SNR. At the same time, due to the improvement in the DOA estimates, the interference term also diminishes. In the simulations, the sources are widely separated. As the SNR increases to as low as 0dB, the SAR has been around 5 dB. The SAR and SIR have already become similar, which means that the interference term has become significantly small. Therefore, the SDR and SAR

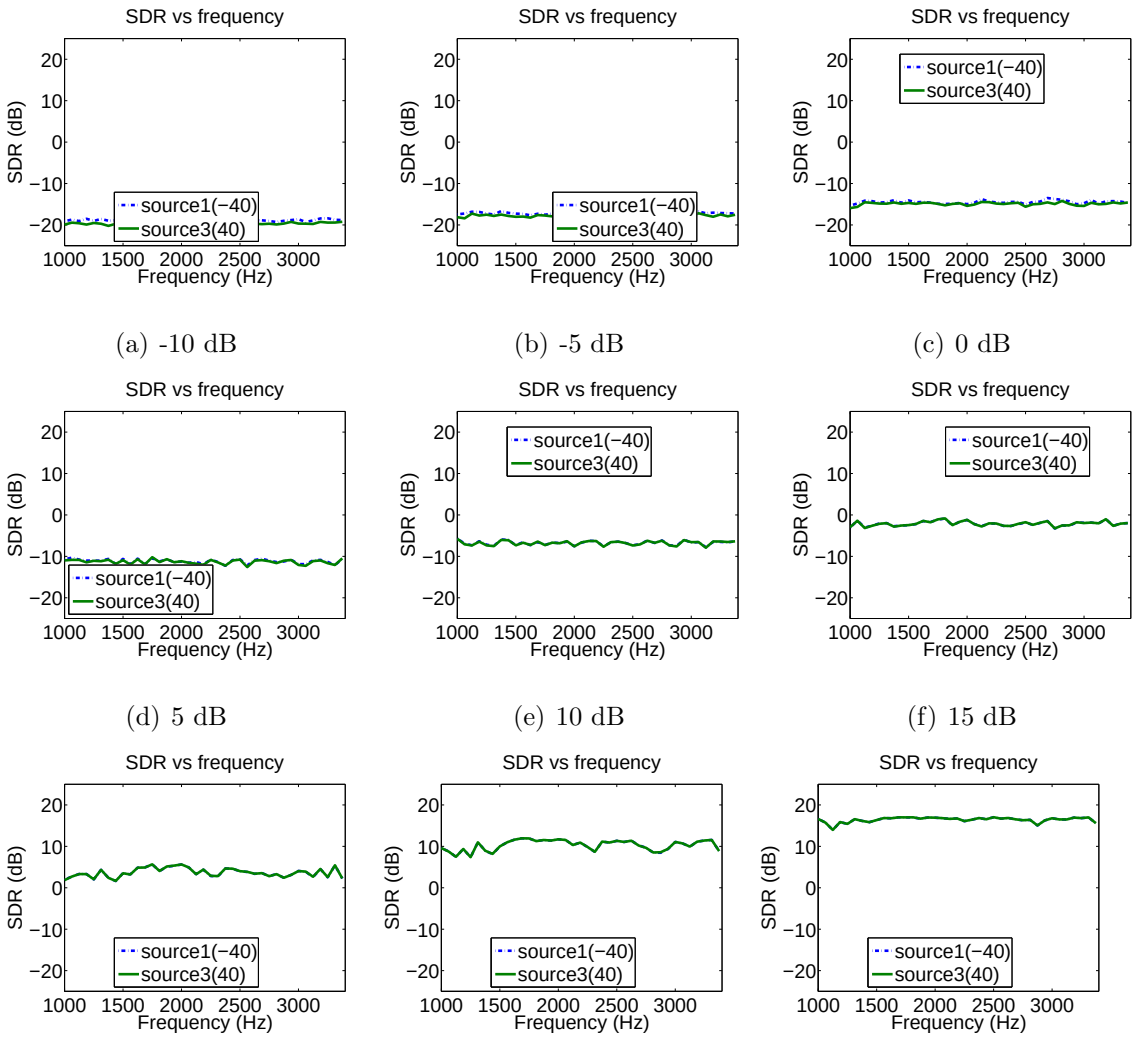

(a) -10 dB (b) -5 dB (c) 0 dB

(d) 5 dB (e) 10 dB (f) 15 dB

(g) 20 dB (h) 25 dB (i) 30 dB

Figure 4.8: SDR versus frequency at different SNRs using Source1 and Source3.

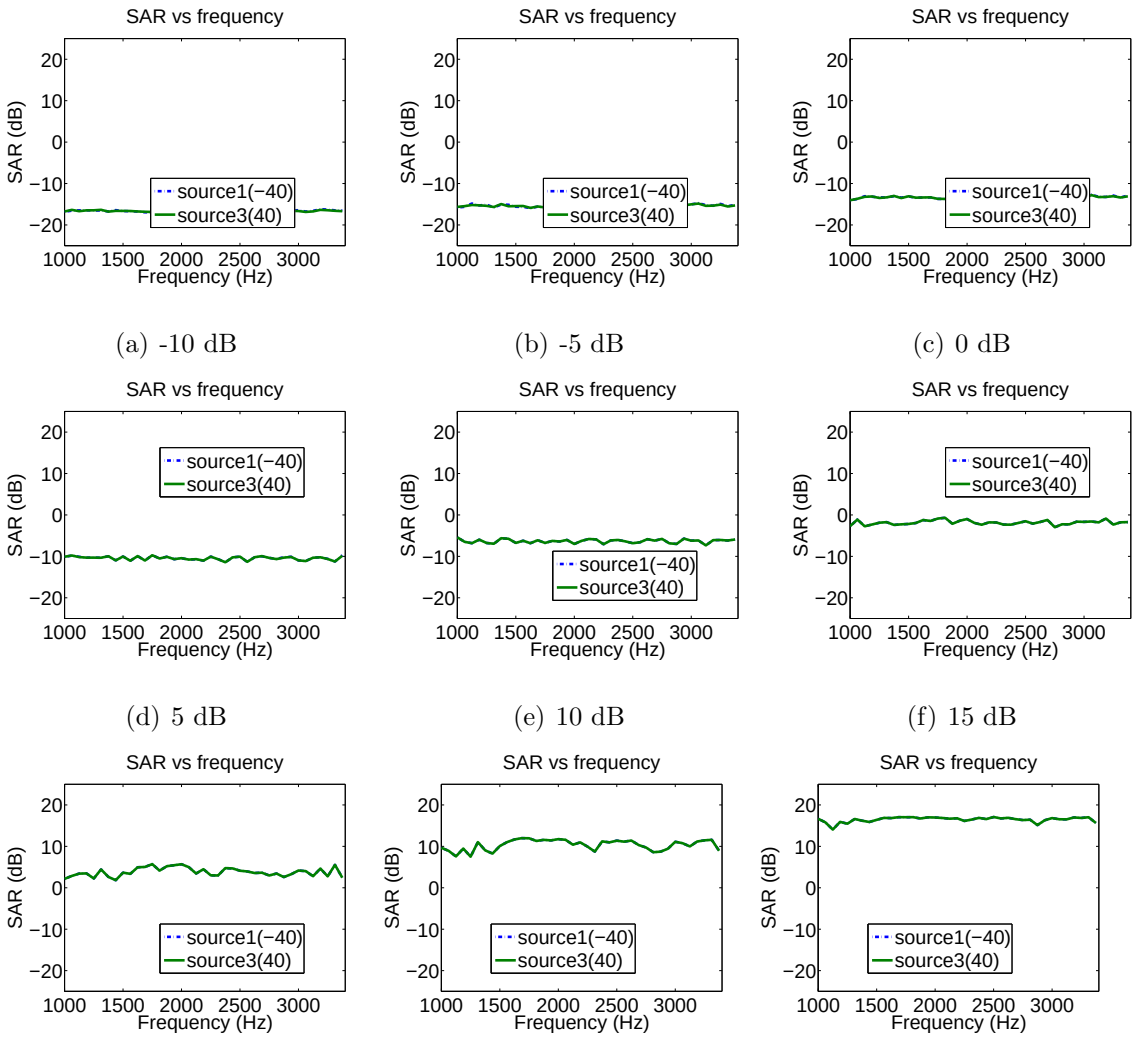

(a) -10 dB (b) -5 dB (c) 0 dB

(d) 5 dB (e) 10 dB (f) 15 dB

(g) 20 dB (h) 25 dB (i) 30 dB

Figure 4.9: SAR versus frequency at different SNRs using Source1 and Source3.

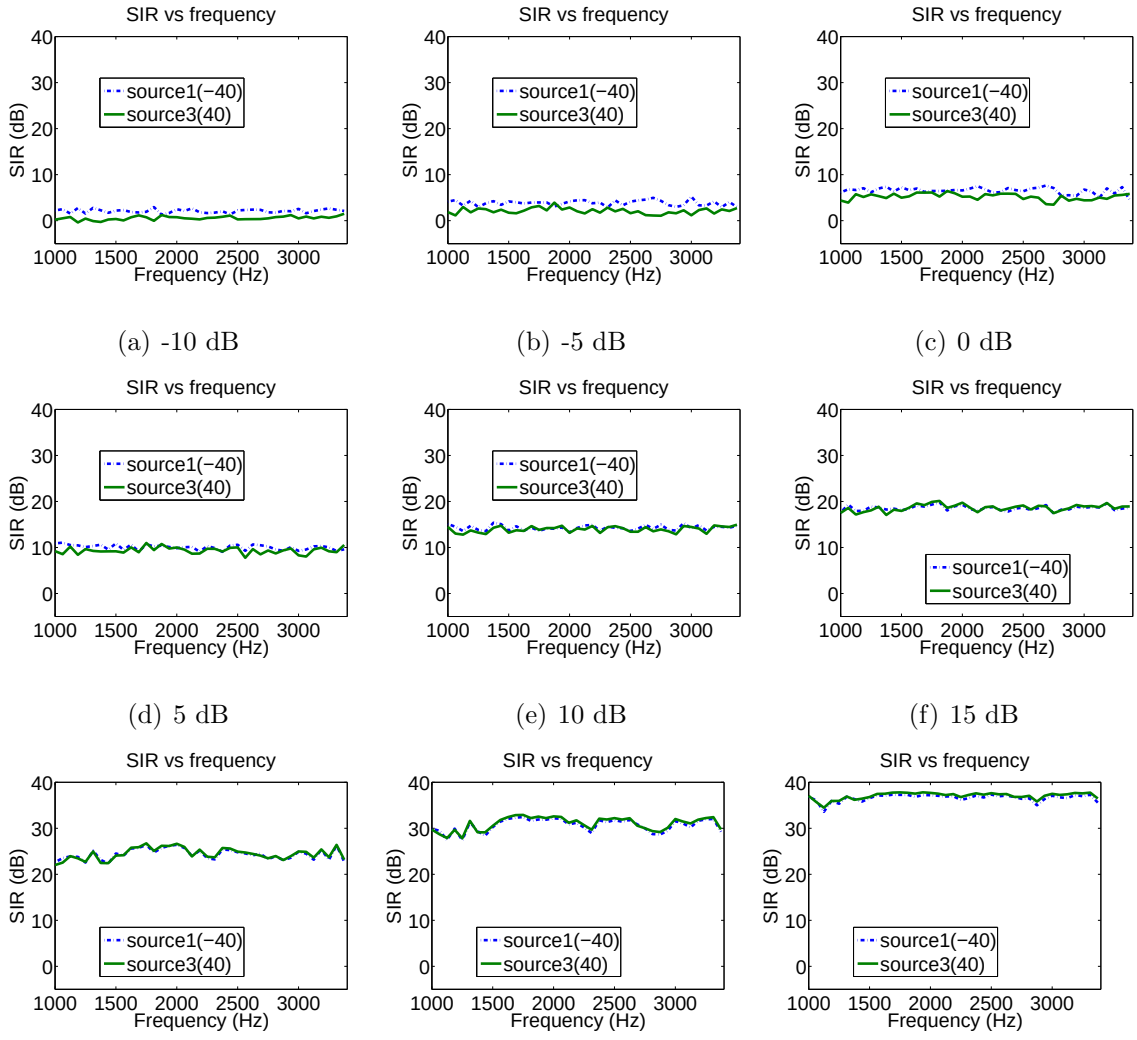

(a) -10 dB (b) -5 dB (c) 0 dB

(d) 5 dB (e) 10 dB (f) 15 dB

(g) 20 dB (h) 25 dB (i) 30 dB

Figure 4.10: SIR versus frequency at different SNRs using Source1 and Source3.

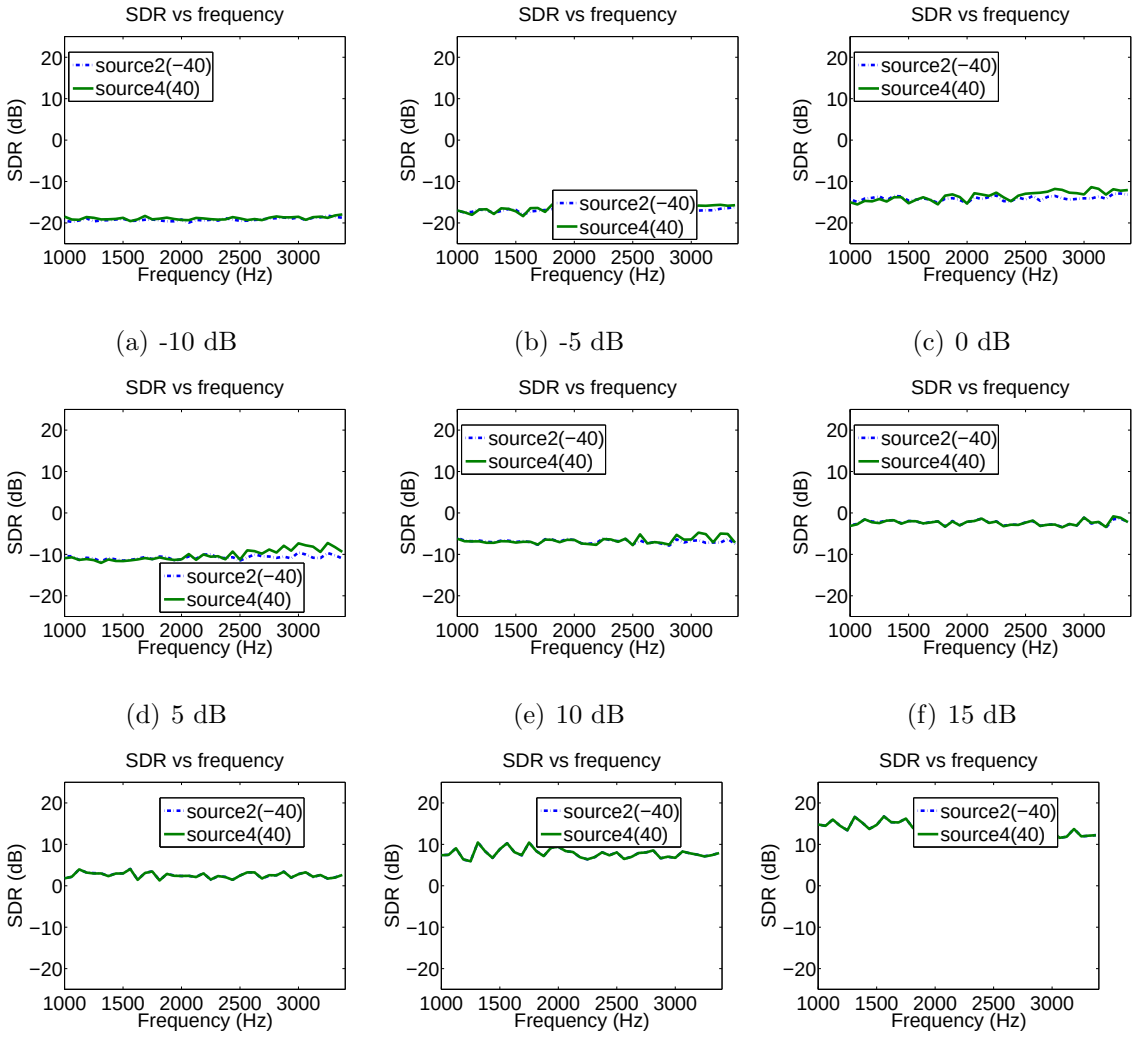

(a) -10 dB (b) -5 dB (c) 0 dB

(d) 5 dB (e) 10 dB (f) 15 dB

(g) 20 dB (h) 25 dB (i) 30 dB

Figure 4.11: SDR versus frequency at different SNRs using Source2 and Source4.

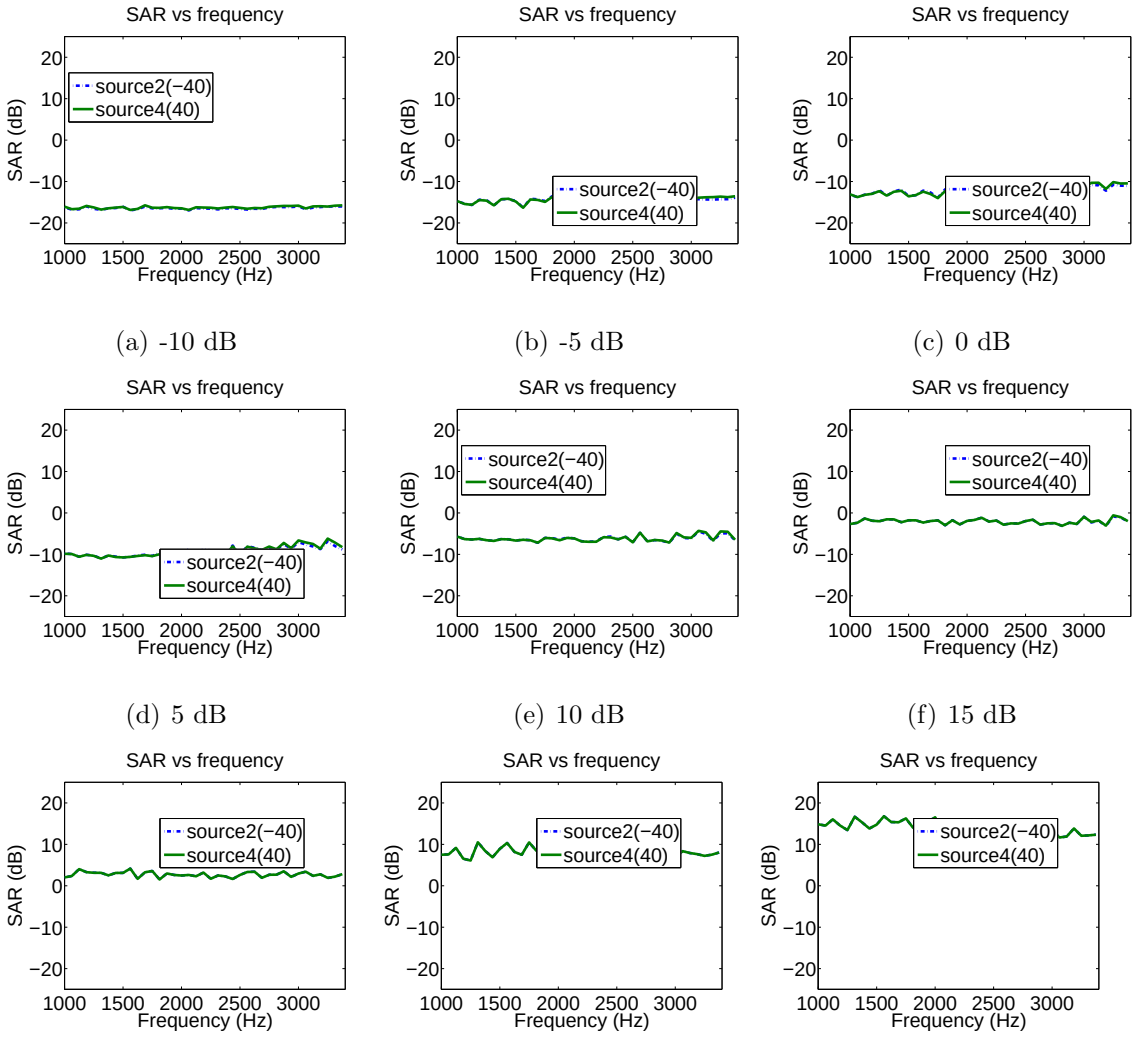

(a) -10 dB (b) -5 dB (c) 0 dB

(d) 5 dB (e) 10 dB (f) 15 dB

(g) 20 dB (h) 25 dB (i) 30 dB

Figure 4.12: SAR versus frequency at different SNRs using Source2 and Source4.

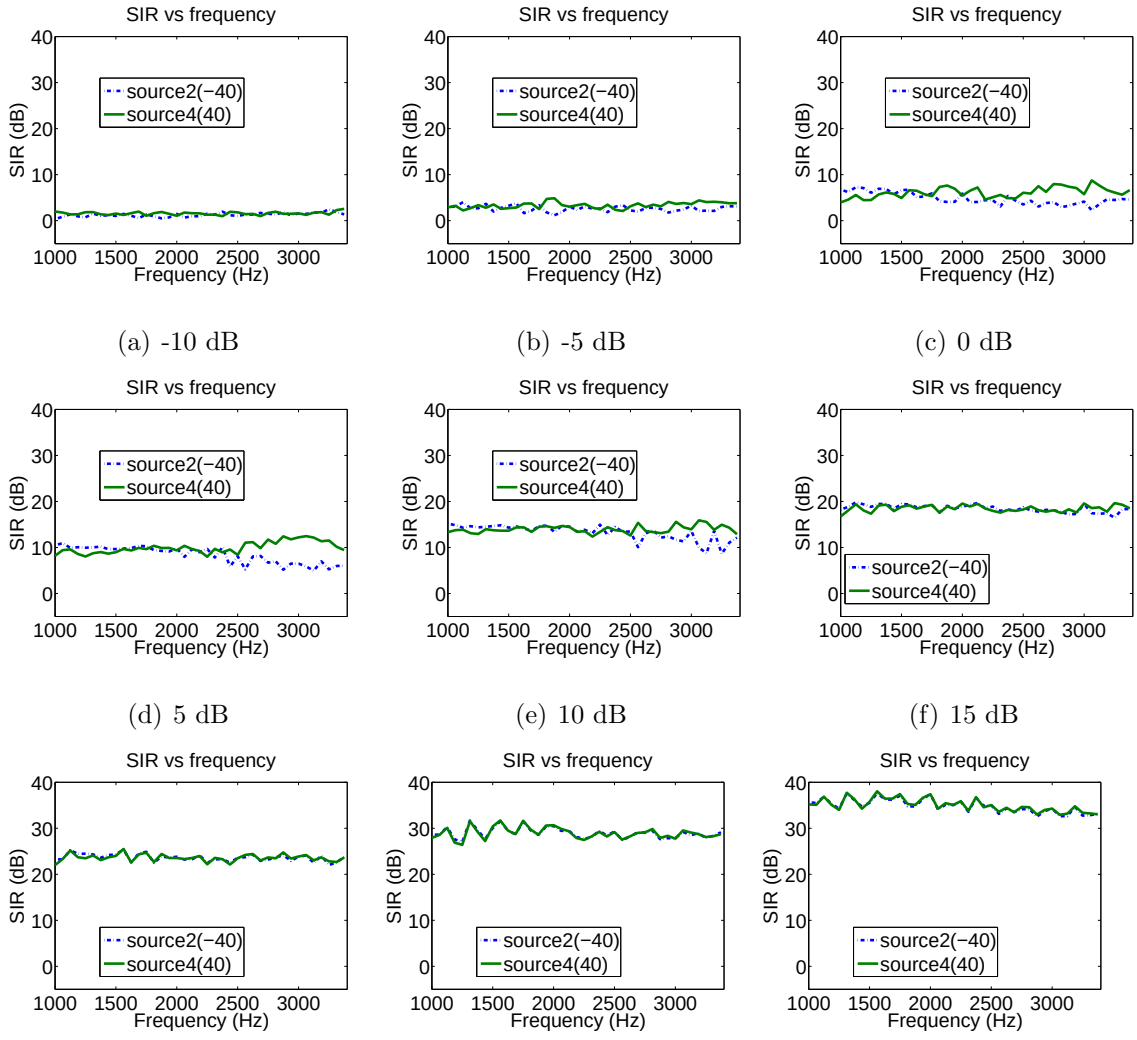

(a) -10 dB (b) -5 dB (c) 0 dB

(d) 5 dB (e) 10 dB (f) 15 dB

(g) 20 dB (h) 25 dB (i) 30 dB

Figure 4.13: SIR versus frequency at different SNRs using Source2 and Source4.

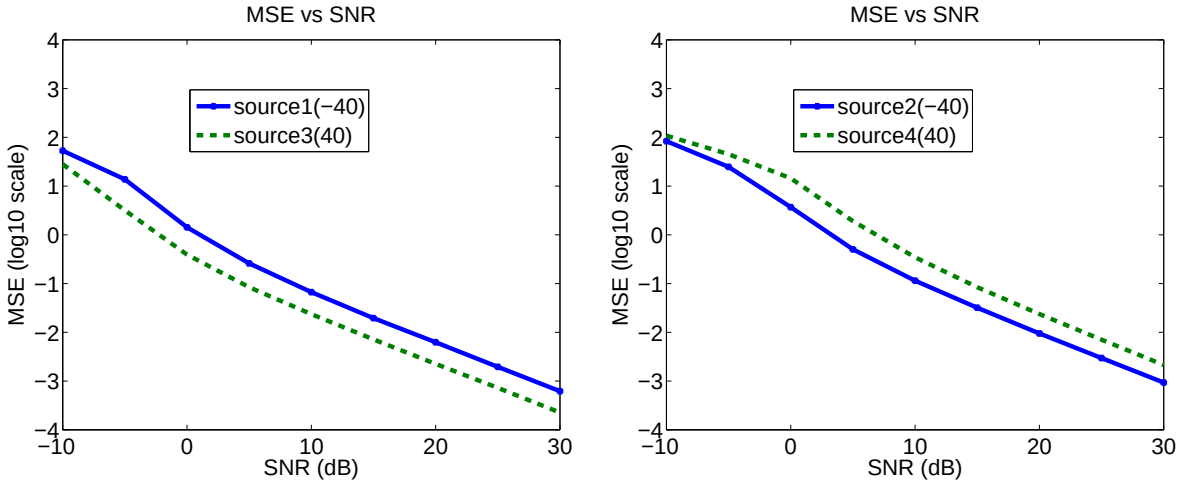

(a) Mixtures of Source1 and Source3 (b) Mixtures of Source2 and Source4

Figure 4.14: MSE versus SNR using the average of DOA estimates for different source combinations.

formulas become quite close to each other. As the SNR becomes about 30 dB, the SIR is extremely large, and the SAR and SIR are extremely similar. All of these observations corroborate the idea of beamforming or spatial filtering.

4.1.5 θ_m Estimation and Associated Separation

θ_m Estimation Performance

Figures 4.14 and 4.15 show the MSE of DOA estimates versus SNR using the average and weighted average. Basically, these two methods have similar localization performance. It is obvious that for different source combinations and two different DOA determination methods, better localization is achieved with increasing SNRs.

Separation Performance

Figures 4.16 and 4.18 show how the SDR, SIR, and SAR change with SNR using the average and weighted average for mixture of Source1 and Source3. Figures 4.17 and 4.19 show the results for mixture of Source2 and Source4. Similar to the local-

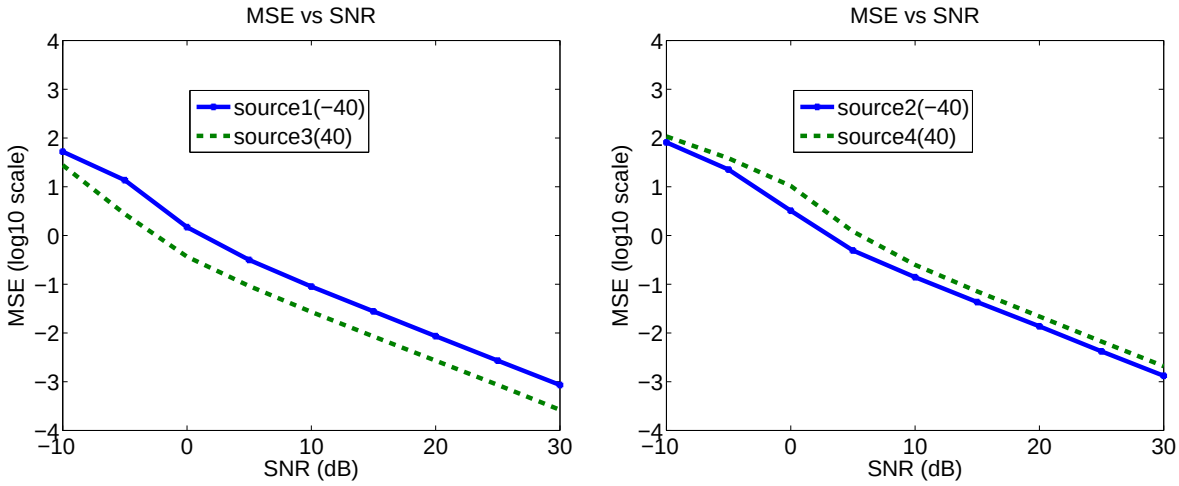

(a) Mixtures of Source1 and Source3 (b) Mixtures of Source2 and Source4

Figure 4.15: MSE versus SNR using the weighted average of DOA estimates for different source combinations.

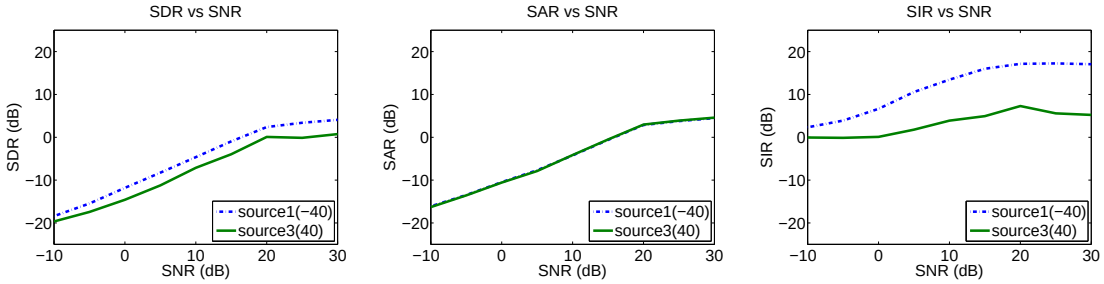

(a) SDR vs SNR (b) SAR vs SNR (c) SIR vs SNR

Figure 4.16: SDR, SAR, and SIR versus SNR using the average of DOA estimates for mixture of Source1 and Source3.

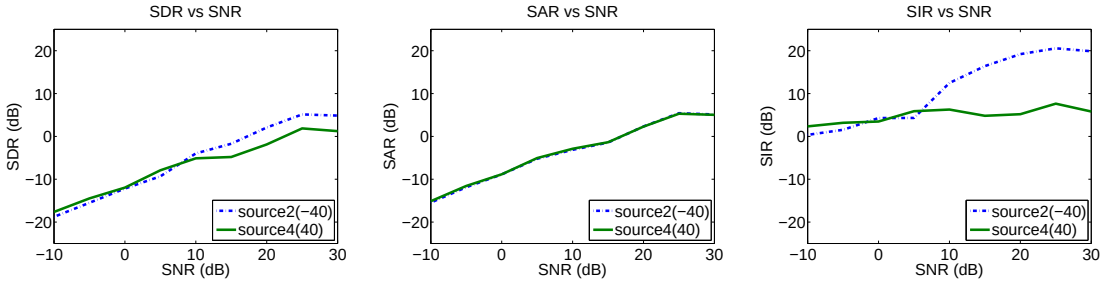

(a) SDR vs SNR (b) SAR vs SNR (c) SIR vs SNR

Figure 4.17: SDR, SAR, and SIR versus SNR using the average of DOA estimates for mixture of Source2 and Source4.

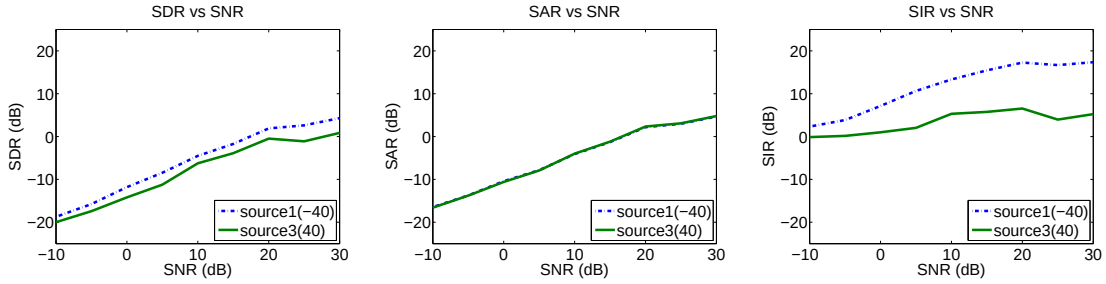

(a) SDR vs SNR (b) SAR vs SNR (c) SIR vs SNR

Figure 4.18: SDR, SAR, and SIR versus SNR using the weighted average of DOA estimates for mixture of Source1 and Source3.

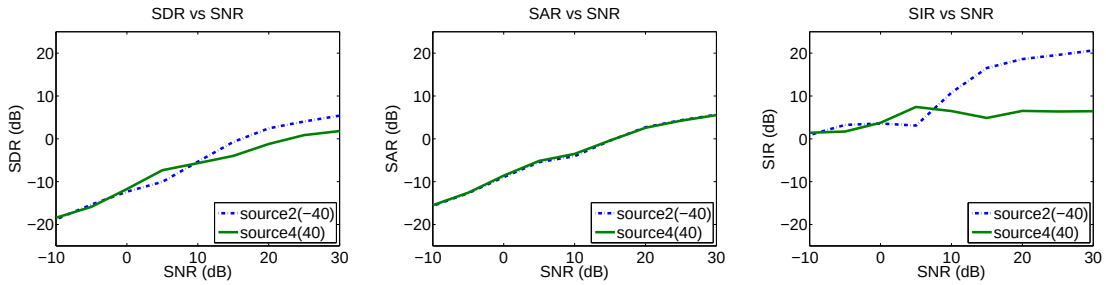

(a) SDR vs SNR (b) SAR vs SNR (c) SIR vs SNR

Figure 4.19: SDR, SAR, and SIR versus SNR using the weighted average of DOA estimates for mixture of Source2 and Source4.

Table 4.2: Parameter setting for comparison.

Parameters	Values
Number of arrays U	2
Number of sources M	2
Number of microphone on each array R	5
Time duration	4 seconds
Inter-microphone spacing d	0.05 m
Velocity of sound c	340 m/s
Frame length	1024
Frame shift	1024
Sampling rate F_s	16 kHz
Window function	Rectangular or Hanning window
Lower frequency threshold	1 kHz
Chosen frequency percentage	30%

ization performance, the separation performance improves with increasing SNRs, due to more accurate DOA estimates.

4.1.6 Source Coordinate Estimation and Separation using Multiple Arrays

We compare our method with Nion's method in two ways. One is to use the same array configuration for these two methods. The other is to use the array configuration for our algorithm and an arbitrary configuration for Nion's method. Table 4.2 summarizes the parameter setting for comparison.

Table 4.3: Comparison with Nion's method.

	Our method	Nion's method
Localization	DOA	TDOA
Microphone placement	Array	Arbitrary
Attenuation coefficients	Uniform (far field)	Arbitrary
Real-time implementation	$\surd$	$\times$
Absolute time mixture	$\surd$	separation ($\surd$) & localization ($\times$)
Absolute frequency mixture	$\surd$	separation ($\surd$) & localization ($\times$)
Relative time mixture	$\surd$	separation ($\surd$) & localization ($\times$)
Relative frequency mixture	$\surd$	separation ($\surd$) & localization ($\times$)

With the Same Array Configuration for the two methods

Figure 4.20 shows the spatial configuration of microphone arrays and sources. Table 4.3 gives the comparison of our method and Nion's method.

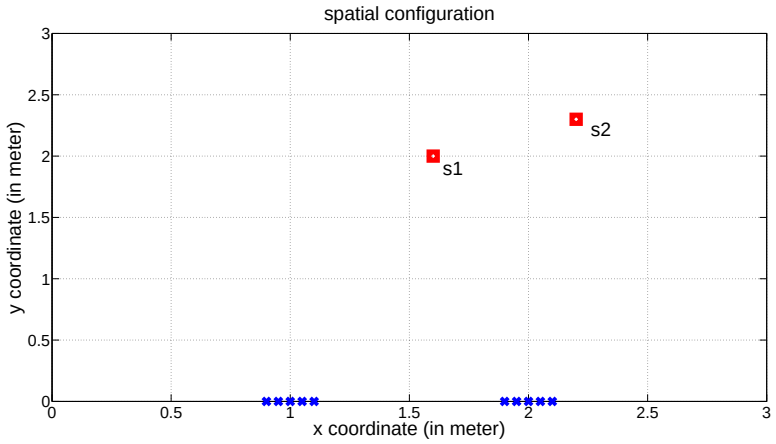

Figure 4.20: Spatial configuration for algorithm comparison.

Nion's method works in separation and fails in localization for all four kinds of mixtures. The reason may be the relatively special locations of the microphones. To

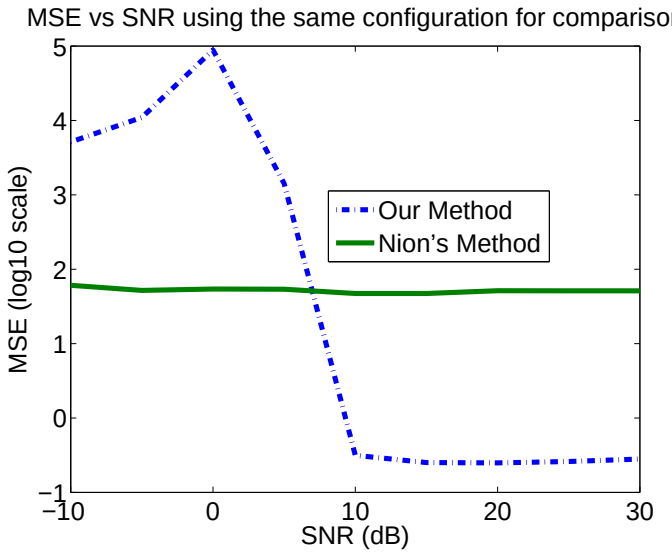

Figure 4.21: MSE vs SNR using two methods for the same configuration.

be more specific, the microphones are on parallel linear arrays. Moreover, the spacing is small and so are the corresponding delays. The microphone signals on the same array experience the spatial aliasing.

For our algorithm, if time domain mixtures are used, the performance of the algorithm using a Hanning window is much better than the performance when using a rectangular window. A rectangular window has a high peak side lobe value, which means that the ringing effect is significant, and a wide main lobe, indicating its large smoothing effect. On the other hand, a Hanning window has a relatively narrower main lobe and a lower peak side lobe value. Therefore, its smoothing effect and ringing effect are both less significant than a rectangular window. All of these are related to the spectral leakage of a finite discrete Fourier transform (DFT) window.

By using absolute delay mixtures in the time domain, we compare the separation and localization performance of these two methods. Figure 4.21 shows the MSE of source coordinate estimates at different SNRs. Our algorithm generally has a decreasing MSE as the SNR increases. However, Nion's method gives a constant MSE. It should be emphasized that the MSE performance of these two methods at

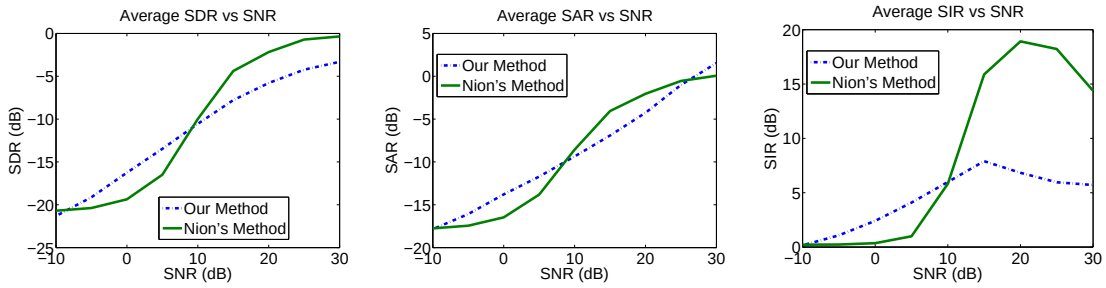

(a) SDR vs SNR (b) SAR vs SNR (c) SIR vs SNR

Figure 4.22: SDR, SAR, SIR versus SNR using two methods for the same configuration.

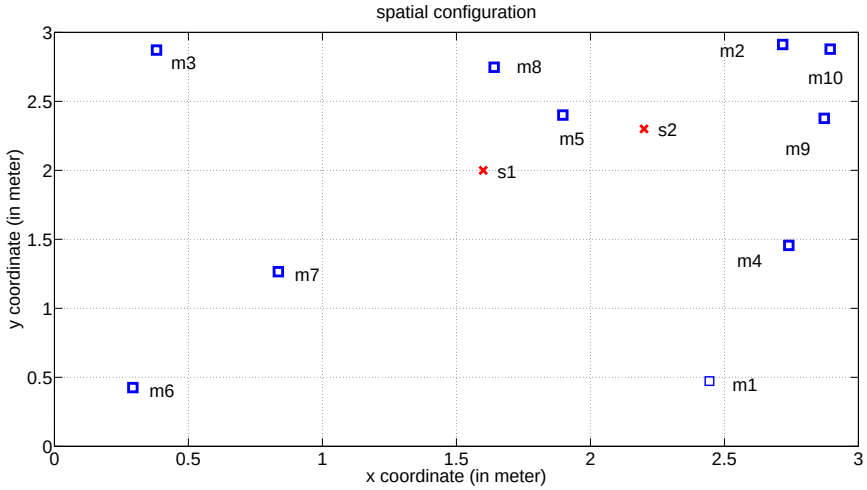

Figure 4.23: Spatial configuration for Nion's method.

low SNRs is extremely bad.

Figure 4.22 shows how the SDR, SAR, and SIR change with SNR using these two methods. It is clear that two algorithms are close in the separation performance. Specifically, at lower SNRs, our algorithm is a little better in all SDR, SAR, and SIR, while Nion's method becomes better in SDR, SAR, and SIR at higher SNRs. As to why the SIR for our algorithm becomes worse for large SNRs, it is subject to a further exploration.

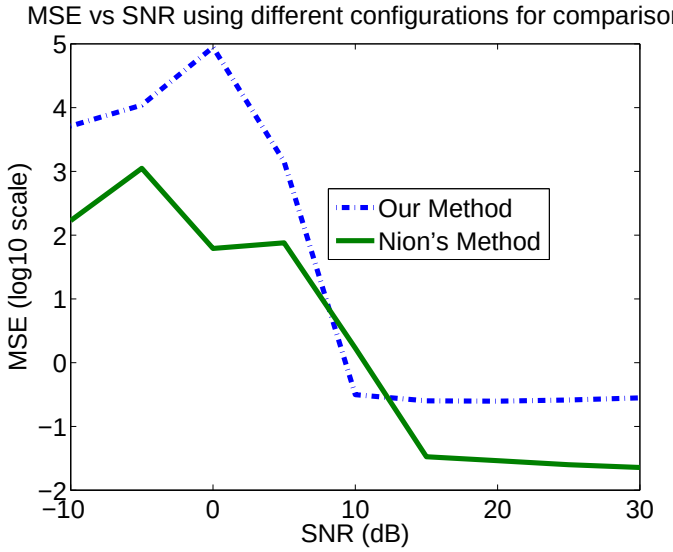

Figure 4.24: MSE vs SNR using two methods for different configurations.

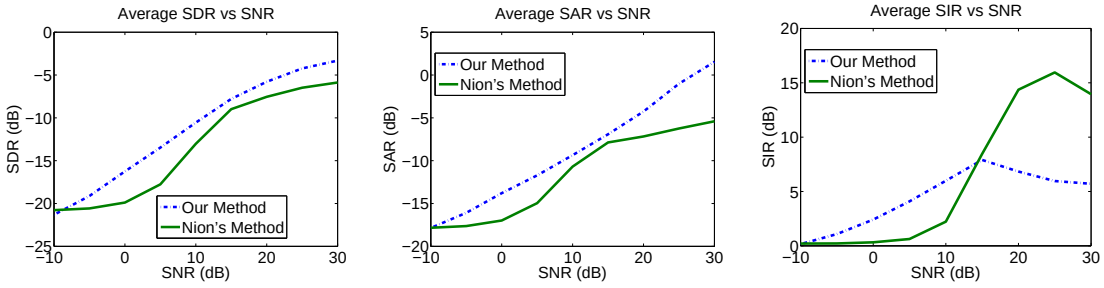

(a) SDR vs SNR (b) SAR vs SNR (c) SIR vs SNR

Figure 4.25: SDR, SAR, SIR versus SNR using two methods for different configurations.

With Different Configurations for the two methods

Our algorithm still uses the same configuration as shown in Figure 4.20, while for Nion's method, an arbitrary microphone placement as shown in Figure 4.23 is used. That is, 10 microphones are randomly placed in a 3×3 area. Figure 4.24 shows the MSE comparison results of source coordinate estimation. Nion's method performs better than ours in source localization. When the microphones are arbitrarily placed, the relative delays among different source and microphone pairs tend to become large. Therefore, the rounding error due to the sampling rate is relatively smaller and its effect becomes less significant. Therefore, the localization performance of Nion's method using an arbitrary microphone placement becomes better. In other words, although the two MSE curves become flat after certain points, the MSE of Nion's method achieves a lower level due to smaller biases in the relative delays.

Figure 4.25 shows the SDR, SAR, and SIR values using these two methods at different SNRs. It shows that the separation performance of our algorithm is generally better than Nion's method. Basically, the separation and localization performance of Nion's method isn't as closely related to each other as our method. Using the array configuration, Nion's method fails in the localization, while is still able to separate the sources and its performance is close to ours. However, when it has a better localization performance than ours using an arbitrary microphone placement, its localization performance is still inferior to ours most of the time.

4.2 Outdoor Experiments

This section uses real world experiments to test various aspects of our algorithm for outdoor environments.

Figure 4.26: An NI cDAQ 9171 USB chassis and four microphones.

4.2.1 Experimental Description

We perform the experiments in an open area between two buildings. A rectangular wooden frame is used to support four microphones forming an array. We use an NI cDAQ 9171 USB chassis, shown in Figure 4.26, to connect four microphones with a laptop. The microphones are omnidirectional and the highest sampling rate is 51.2 kHz. Two USB-powered loud speakers are placed at the same side of the microphone array as the audio sources. After collecting certain length of signals, our algorithm is used to estimate the DOAs of the sources. Figure 4.27 illustrates one example of the experiment setup. The main noise source in outdoor environments is wind, which significantly affects the performance of our algorithm. The parameter setting for experiments is summarized in Table 4.4.

4.2.2 Source Number Estimation

Information Theoretical Criteria for Source Number Estimation

Figures 4.28 shows the percentage of correct estimate using AIC and MDL criteria. It is clear that, contrary to the results in simulations, the performance in the experiments is much worse. It might be attributed to two factors. One is the SNR. In real

Figure 4.27: An example of the experimental setup.

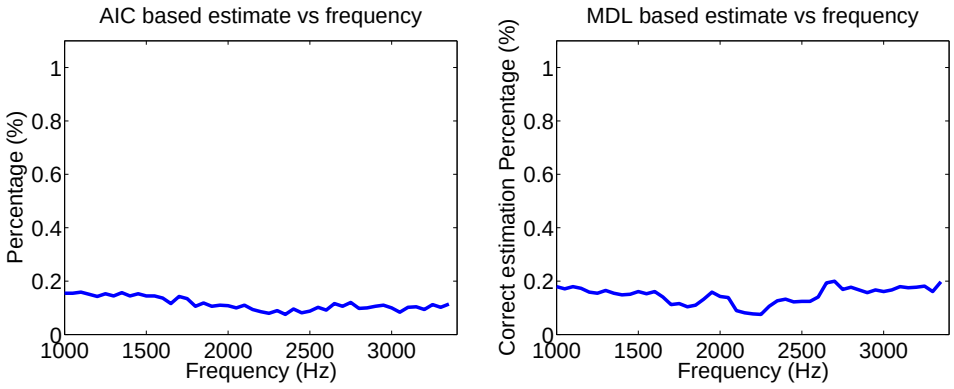

(a) AIC (b) MDL

Figure 4.28: Correct source number estimation percentage versus frequency using AIC and MDL.

Table 4.4: Parameter setting for outdoor experiments.

Experimental Parameters	Values
Number of sources M	2
Source categories	Speech & music
Source length	4 seconds
Number of microphones N	4
Array spacing d	0.05 m
Sampling rate F_s	51.2 kHz
Frame length	1024
Frame shift	1024
FFT window	Rectangular

experiments, the SNRs are unknown and may be quite small. The other is the noise type, which is likely to have more significant influence. The assumption for these two criteria is that the noise is Gaussian in the time domain or circular complex Gaussian in the frequency domain. This may not be the case in real environments, which explains why the methods fail to estimate the source number correctly most of the time.

Eigenvalue Based Source Number Estimation

Figure 4.29 shows the average normalized eigenvalues of the spatial covariance matrix of the collected mixtures. In total, 491 experiment files are used. It is clear that the eigenvalues for signals and noise are well separated, especially at high frequencies. If we have some prior knowledge about the background noise, it is easy to estimate the number of the sources accurately.

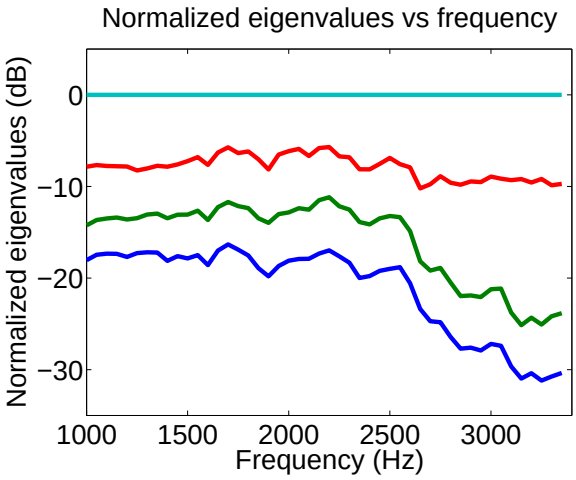

Figure 4.29: Average normalized eigenvalues versus frequency using experimental files.

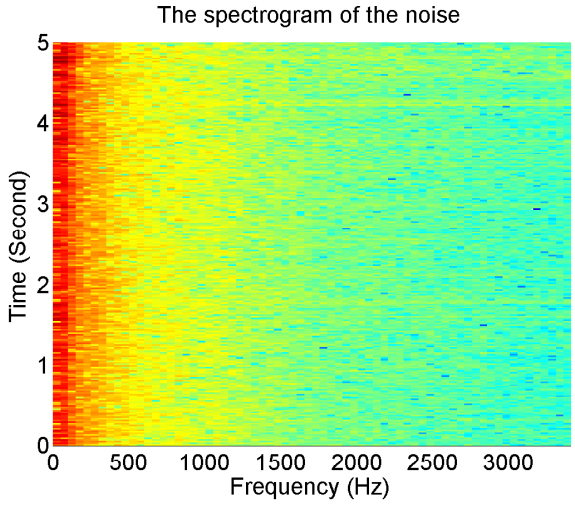

Figure 4.30: The spectrogram of the background noise.

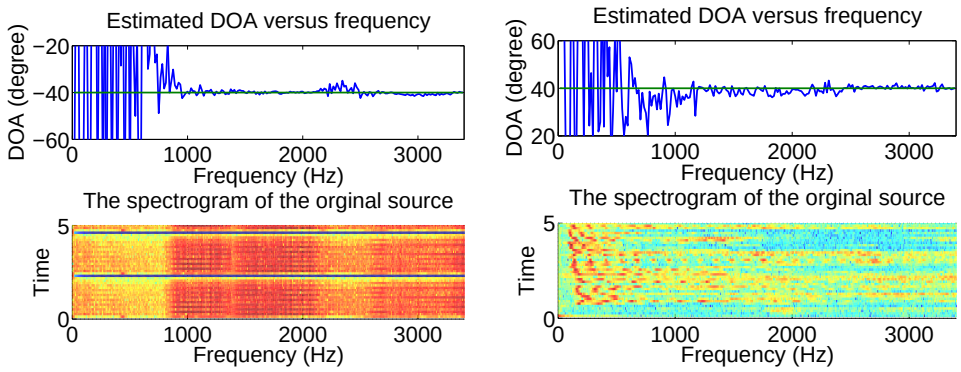

(a) Car siren (b) Male speech

Figure 4.31: Estimated DOAs versus frequency for two sources, and their spectrograms.

4.2.3 Frequency Bin Selection

As in the simulations, we set the lower and upper frequency thresholds, due to the microphone array's inability to capture extremely low frequency signal components and also the spatial aliasing. The algorithm performs DOA estimates using the mixture components in the resulted frequency range. Moreover, environmental noise mainly occupies low frequency range. Figure 4.30 is the spectrogram of the background noise during an experiment. It is clear that most part of the noise power is distributed below 1 kHz.

When signals mostly consist of low frequency components, the algorithm fails to give good estimates because of the low SNRs. When signals includes a significant amount of high frequency components, the estimates at these frequencies are relatively accurate. Figure 4.31 shows the DOA estimate versus frequency for two sources and their original source spectrograms. It is noted that except for the low frequency part, the estimated DOAs are more accurate at the frequencies with high power and less accurate at the low frequencies. This is clear in Figure 4.31(a). The performance difference is due to the SNR difference at different frequencies.

CHAPTER 5

CONCLUSIONS AND FUTURE WORK

5.1 Conclusions

A subspace-based audio signal separation and localization scheme has been proposed for pure delay mixtures collected by microphone arrays. The algorithm applies the STFT to the mixtures and uses the subspace methods, such as MUSIC and ESPRIT, to estimate the DOAs of audio sources at each frequency independently. The DOA estimates at frequencies with large SSA values are combined to obtain the final DOA estimates. Correspondingly, the mixing and demixing matrices are computed, and the source signals are recovered using the inverse STFT.

The algorithm is robust to noise at the cost of more microphones than sources. Also, the permutation issue does not exist for our algorithm. Our localization-based separation approach is essentially a beamformer, which extracts the signals at estimated DOAs from collected mixtures. Moreover, it supports real-time implementation. That is, the required signal length is generally short. Unlike optimization-based source separation methods, it directly gives the DOA estimates and in turn the demixing matrices, and does not resort to iterative computations. We have discussed several crucial issues closely related to the algorithm and their solutions, including source number estimation, spatial aliasing, different ways of mixture generation, frequency bin selection, and artifact filtering. Both simulations and experiments have been conducted to test the effectiveness and performance of the algorithm.

5.2 Future Work

In the future, we intend to consider the sound localization and separation problem in more challenging and realistic indoor reverberant environments as well as the underdetermined and critically determined scenarios. We will also try to develop new methods applicable for real world experiments, while taking the current state-of-the-art methods into consideration.

BIBLIOGRAPHY

[1] D. Nion, B. Vandewoestyne, S. Vanaverbeke, K. Van Den Abeele, H. De Gersem, and L. De Lathauwer, *A Time-Frequency Technique for Blind Separation and Localization of Pure Delayed Sources Latent Variable Analysis and Signal Separation*, vol. 6365 of *Lecture Notes in Computer Science*, pp. 546–554. Springer Berlin / Heidelberg, 2010.

[2] S. Makeig, A. J. Bell, T. ping Jung, and T. J. Sejnowski, "Independent component analysis of electroencephalographic data," in *in Advances in Neural Information Processing Systems*, pp. 145–151, MIT Press, 1996.

[3] E. C. Cherry, "Some experiments on the recognition of speech, with one and with two ears," *Journal of the Acoustical Society of America*, vol. 25, no. 5, p. 5, 1953.

[4] K. Kokkinakis and P. C. Loizou, "Using blind source separation techniques to improve speech recognition in bilateral cochlear implant patients," *Journal of the Acoustical Society of America*, vol. 123, no. 4, p. 12, 2008.

[5] M. Sahiduilah and G. Saha, "Design, analysis and experimental evaluation of block based transformation in mfcc computation for speaker recognition," *Speech Communication*, vol. 54, no. 4, pp. 543–565, 2012.

[6] M. D. Plumbley, S. A. Abdallah, J. P. Bello, M. E. Davies, G. Monti, and M. B. Sandler, "Automatic music transcription and audio source separation," 2001.

[7] M. Brandstein and D. E. Ward, *Microphone arrays: signal processing techniques and applications*. Springer-Verlag Berlin, 2001.

[8] J. Dmochowski, J. Benesty, and S. Affes, "On spatial aliasing in microphone arrays," *Signal Processing, IEEE Transactions on*, vol. 57, no. 4, pp. 1383–1395, 2009.

[9] V. C. Chen and L. Hao, "Joint time-frequency analysis for radar signal and image processing," *Signal Processing Magazine, IEEE*, vol. 16, no. 2, pp. 81–93, 1999.

[10] A. Hyvarinen and E. Oja, "Independent component analysis: algorithms and applications," *Neural Netw.*, vol. 13, no. 4-5, pp. 411–430, 2000.

[11] O. Yilmaz and S. Rickard, "Blind separation of speech mixtures via time-frequency masking," *Signal Processing, IEEE Transactions on*, vol. 52, no. 7, pp. 1830–1847, 2004.

[12] D. Wang and G. J. Brown, *Computational Auditory Scene Analysis: Principles, Algorithms, and Applications*. Hoboken, NJ: Wiley, 2006.

[13] M. I. Mandel, R. J. Weiss, and D. Ellis, "Model-based expectation-maximization source separation and localization," *Audio, Speech, and Language Processing, IEEE Transactions on*, vol. 18, no. 2, pp. 382–394, 2010.

[14] A. J. Bell and T. J. Sejnowski, "An information-maximization approach to blind separation and blind deconvolution," *Neural Computation*, vol. 7, pp. 1129–1159, 1995.

[15] P. Smaragdis, "Blind separation of convolved mixtures in the frequency domain," February 9-10 1998.

[16] H. Sawada, S. Araki, and S. Makino, "Measuring dependence of bin-wise separated signals for permutation alignment in frequency-domain bss," in *Circuits and Systems, 2007. ISCAS 2007. IEEE International Symposium on*, pp. 3247–3250, 2007.

[17] H. Sawada, R. Mukai, S. Araki, and S. Makino, "A robust and precise method for solving the permutation problem of frequency-domain blind source separation," *Speech and Audio Processing, IEEE Transactions on*, vol. 12, no. 5, pp. 530–538, 2004.

[18] H. Sawada, S. Araki, and S. Makino, "Underdetermined convolutive blind source separation via frequency bin-wise clustering and permutation alignment," *Audio, Speech, and Language Processing, IEEE Transactions on*, vol. 19, no. 3, pp. 516–527, 2011.

[19] H. Sawada, R. Mukai, and S. Makino, "Direction of arrival estimation for multiple source signals using independent component analysis," in *Signal Processing and Its Applications, 2003. Proceedings. Seventh International Symposium on*, vol. 2, pp. 411–414 vol.2, 2003.

[20] S. Kurita, H. Saruwatari, S. Kajita, K. Takeda, and F. Itakura, "Evaluation of blind signal separation method using directivity pattern under reverberant conditions," in *Acoustics, Speech, and Signal Processing, 2000. ICASSP '00. Proceedings. 2000 IEEE International Conference on*, vol. 5, pp. 3140–3143 vol.5, 2010.

[21] Y. Li, S.-I. Amari, A. Cichocki, D. Ho, and S. Xie, "Underdetermined blind source separation based on sparse representation," *IEEE Transactions on Signal Processing*, vol. 54, no. 2, pp. 423 – 437, 2006.

[22] E. Vincent, S. Araki, F. Theis, G. Nolte, P. Bofill, H. Sawada, A. Ozerov, V. Gowreesunker, D. Lutter, and N. Q. K. Duong, "The signal separation evaluation campaign (20072010): Achievements and remaining challenges," *Signal Processing*, vol. 92, no. 8, pp. 1928–1936, 2012.

[23] A. Ozerov and C. Fevotte, "Multichannel nonnegative matrix factorization in convolutive mixtures for audio source separation," *Audio, Speech, and Language Processing, IEEE Transactions on*, vol. 18, no. 3, pp. 550–563, 2010.

[24] P. Aarabi, "Self-localizing dynamic microphone arrays," *Systems, Man, and Cybernetics, Part C: Applications and Reviews, IEEE Transactions on*, vol. 32, no. 4, pp. 474–484, 2002.

[25] Z. Wenyi and B. D. Rao, "A two microphone-based approach for source localization of multiple speech sources," *Audio, Speech, and Language Processing, IEEE Transactions on*, vol. 18, no. 8, pp. 1913–1928, 2010.

[26] R. Schmidt, "Multiple emitter location and signal parameter estimation," *Antennas and Propagation, IEEE Transactions on*, vol. 34, no. 3, pp. 276–280, 1986.

[27] R. Roy and T. Kailath, "Esprit-estimation of signal parameters via rotational invariance techniques," *Acoustics, Speech and Signal Processing, IEEE Transactions on*, vol. 37, no. 7, pp. 984–995, 1989.

[28] H. Buchner, R. Aichner, and W. Kellermann, *TRINICON-based Blind System Identification with Application to Multiple-Source Localization and Separation Blind Speech Separation*, pp. 101–147. Signals and Communication Technology, Springer Netherlands, 2007.

[29] T. May, S. van de Par, and A. Kohlrausch, "A binaural scene analyzer for joint localization and recognition of speakers in the presence of interfering noise sources and reverberation," *Audio, Speech, and Language Processing, IEEE Transactions on*, vol. 20, no. 7, pp. 2016–2030, 2012.

[30] T. May, S. van de Par, and A. Kohlrausch, "A probabilistic model for robust localization based on a binaural auditory front-end," *Audio, Speech, and Language Processing, IEEE Transactions on*, vol. 19, no. 1, pp. 1–13, 2011.

[31] F. Asano, S. Hayamizu, T. Yamada, and S. Nakamura, "Speech enhancement based on the subspace method," *Speech and Audio Processing, IEEE Transactions on*, vol. 8, no. 5, pp. 497–507, 2000.

[32] P. Stoica and T. Soderstrom, "Statistical analysis of music and subspace rotation estimates of sinusoidal frequencies," *Trans. Sig. Proc.*, vol. 39, no. 8, pp. 1836–1847, 1991.

[33] H. Akaike, "A new look at the statistical model identification," *Automatic Control, IEEE Transactions on*, vol. 19, no. 6, pp. 716–723, 1974.

[34] J. Rissanen, "Modeling by shortest data description," *Automatica*, vol. 14, no. 5, pp. 465–471, 1978.

[35] G. Schwarz, "Estimating the dimension of a model," *Annals of Statistics*, vol. 6, p. 4, 1978.

[36] M. Wax and T. Kailath, "Detection of signals by information theoretic criteria," *Acoustics, Speech and Signal Processing, IEEE Transactions on*, vol. 33, no. 2, pp. 387–392, 1985.

[37] S. Winter, H. Sawada, and S. Makino, "Geometrical interpretation of the pca subspace approach for overdetermined blind source separation," *EURASIP J. Appl. Signal Process.*, vol. 2006, pp. 176–176, 2006.

[38] E. Vincent, R. Gribonval, and C. Fevotte, "Performance measurement in blind audio source separation," *Audio, Speech, and Language Processing, IEEE Transactions on*, vol. 14, no. 4, pp. 1462–1469, 2006.

[39] C. Fevotte, R. Gribonval, and E. Vincent, "Bss_eval toolbox user guide." `http://www.irisa.fr.metiss/bss\_eval`, 2005.

[40] H. Wang and M. Kaveh, "Coherent signal-subspace processing for the detection and estimation of angles of arrival of multiple wide-band sources," *Acoustics, Speech and Signal Processing, IEEE Transactions on*, vol. 33, no. 4, pp. 823–831, 1985.

[41] L. Chang; and C.-F. Twu;, "The estimation of direction-of-arrival of wideband sources by signal subspace focusing approach," *Journal of Marine Science and Technology*, vol. 6, no. 1, pp. 9–15, 1998.

[42] Y.-S. Yoon, *Direction-of-arrival estimation of wideband sources using sensor arrays*. PhD thesis, 2004.

VITA

Longji Sun

Candidate for the Degree of

Master of Science

Thesis: BLIND SOURCE SEPARATION AND LOCALIZATION USING MICROPHONE ARRAYS

Major Field: Electrical Engineering

Biographical:

Personal Data: Born in Dengzhou, Henan, China, on December 3rd, 1988.

Education:

Received the Bachelor of Engineering (B.E.) degree from University of Shanghai for Science and Technology, Shanghai, China, 2010, in Communication Engineering

Completed the requirements for the degree of Master of Science (M.S.) with a major in Electrical Engineering from Oklahoma State University in December, 2012.

Experience:

Research assistant, School of Electrical and Computer Engineering, Oklahoma State University, 08/2010-present

Professional Memberships:

Institute of Electrical and Electronics Engineers (IEEE)

The Honor Society of Phi Kappa Phi

Name: Longji Sun Date of Degree: December, 2012

Institution: Oklahoma State University Location: Stillwater, Oklahoma

Title of Study: BLIND SOURCE SEPARATION AND LOCALIZATION USING MICROPHONE ARRAYS

Pages in Study: 66 Candidate for the Degree of Master of Science

Major Field: Electrical Engineering

The blind source separation and localization problem for audio signals is studied using microphone arrays. Pure delay mixtures of source signals typically encountered in outdoor environments are considered. Our proposed approach utilizes the subspace methods, including multiple signal classification (MUSIC) and estimation of signal parameters via rotational invariance techniques (ESPRIT) algorithms, to estimate the directions of arrival (DOAs) of the sources from the collected mixtures. Since audio signals are generally considered broadband, the DOA estimates at frequencies with the large sum of squared amplitude values are combined to obtain the final DOA estimates. Using the estimated DOAs, the corresponding mixing and demixing matrices are computed, and the source signals are recovered using the inverse short time Fourier transform.

Subspace methods take advantage of the spatial covariance matrix of the collected mixtures to achieve robustness to noise. While the subspace methods have been studied for localizing radio frequency signals, audio signals have their special properties. For instance, they are nonstationary, naturally broadband and analog. All of these make the separation and localization for the audio signals more challenging. Moreover, our algorithm is essentially equivalent to the beamforming technique, which suppresses the signals in unwanted directions and only recovers the signals in the estimated DOAs.

Several crucial issues related to our algorithm and their solutions have been discussed, including source number estimation, spatial aliasing, artifact filtering, different ways of mixture generation, and source coordinate estimation using multiple arrays. Additionally, comprehensive simulations and experiments have been conducted to examine various aspects of the algorithm. Unlike the existing blind source separation and localization methods, which are generally time consuming, our algorithm needs signal mixtures of only a short duration and therefore supports real-time implementation.

ADVISOR'S APPROVAL: Dr. Qi Cheng